

We are IntechOpen, the world's leading publisher of Open Access books Built by scientists, for scientists

6,900

Open access books available

186,000

International authors and editors

200M

Downloads

Our authors are among the

154

Countries delivered to

TOP 1%

most cited scientists

12.2%

Contributors from top 500 universities



WEB OF SCIENCE™

Selection of our books indexed in the Book Citation Index
in Web of Science™ Core Collection (BKCI)

Interested in publishing with us?
Contact book.department@intechopen.com

Numbers displayed above are based on latest data collected.
For more information visit www.intechopen.com



Application of Fiber Bragg Grating Sensors in Power Industry

Regina C. S. B. Allil, Marcelo M. Werneck,
Bessie A. Ribeiro and Fábio V. B. de Nazaré

Additional information is available at the end of the chapter

<http://dx.doi.org/10.5772/54148>

1. Introduction

1.1. Application of a Fiber Bragg Grating temperature system in a grid-connected hydrogenerator

The main control parameters in any hydro-electric plant (HEP) or substation is, of course, the current and voltage. The third parameter is the temperature, which is normally a consequence of the current and must be kept under close observation because rises above 100°C may accelerate the aging of insulating materials and conductors or even destroy them [1].

With the idea of decreasing the number of copper wires and consequently decreasing installation and operation costs, we designed a fiber optic temperature sensor for application in large generators. The objective of the system is to cover all temperature monitoring needs of an HEP that would also overcome some of the disadvantages presented by the conventional RTD (resistive temperature detector) network.

This session describes the research, development and operation of an FBG temperature sensor array for hydro-electric generators. The optical fiber sensors system measured temperature at different points of an operational 42.5-MW generator at full power. The results showed feasibility and usefulness of the optical fiber system in power equipment.

1.2. Installation of sensors in the hydroelectric generator

The HEP chosen for this experiment was the 216 MW UHE-Samuel, in the western city of Porto Velho, Brazil. It is located on the Jamari River, a tributary of the Madeira River, which in turn, is one of the major tributaries of the Amazon River. Before being installed, the FBGs were calibrated in the laboratory to find their sensitivities [2].

The machine, which operates at a temperature of around 95°C at full load, needs 24 hours to drop its temperature to about 45°C to make it possible to enter the stator hall to install the optical sensors.

An FBG presents a very small time constant due to its small mass. To protect this sensor and not deteriorate such a valuable parameter, the sensor was loosely inserted inside a thin 10-cm U-form copper tubing to allow good heat transfer between the cooling air and the optical fiber, as shown in Figure 1. The copper tubing which also protects the sensor against strain comes out of and reenters an IP65 polymeric enclosure.

A conventional optical fiber cable connected all six boxes which were installed around the stator winding behind each radiator of the generator. The optical cable was then placed within the existing cable trays along with the other electric cables extending all the way up from the generator to the HEP control room where the optical interrogator and an industrial PC were installed.

The optical interrogation setup consists of a broad band optical source that illuminates all FBGs in the array. The return signal of each FBG is detected by the optical interrogator (Spectral Eye 400-FOS&S) that identifies the center wavelength of each FBG reflection pulse. Using the calibration parameters of each FBG, the optical interrogator calculates and stores the temperatures and communicates with an industrial PC via RS-232 interface.

The PC publishes all data on the company's Intranet and become available to the HEP central software control. Figure 1 shows the box containing one sensor installed inside the stator and Figure 2 shows a block diagram of the generator in detail with the optical cable connecting the six sensors to the interrogation system.

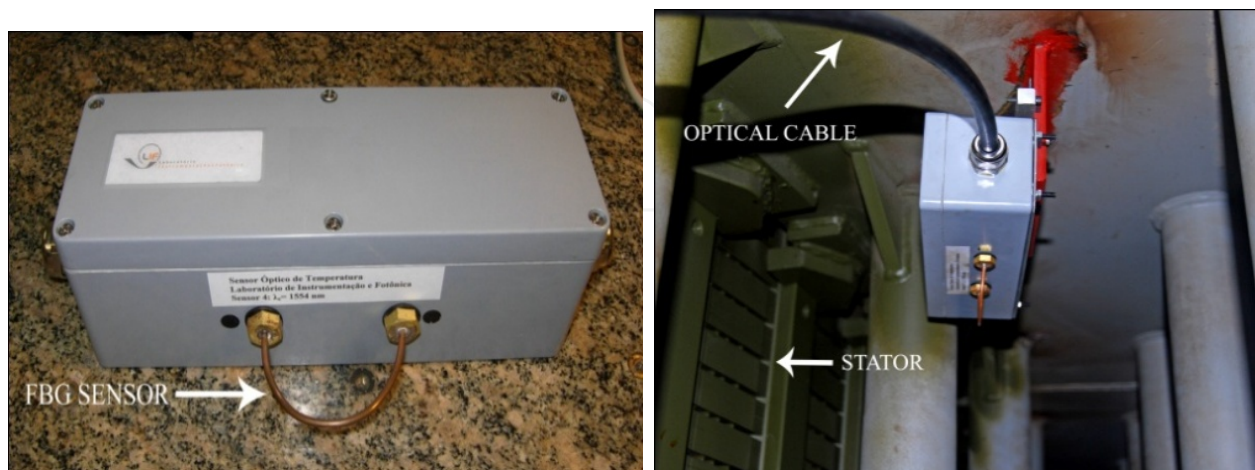


Figure 1. Box containing the optical fiber splices with the FBG inside the U-shape copper tubing (left) and installed inside the generator (right) (adapted from [2]).

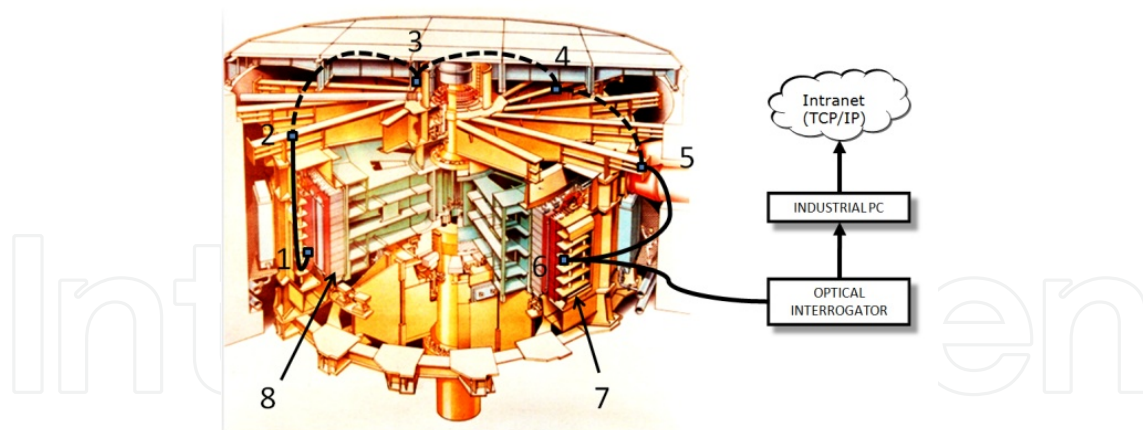


Figure 2. Depiction of a cross-section of the hydrogenerators showing the generator in detail with sensors connected to the interrogation system. 1-6) FBG sensors, 7) Radiator, 8) Stator (adapted from [2]).

1.3. Results

Immediately after the installation, the system started monitoring the temperatures, producing the graph shown in Figure 3. We can observe all signals superimposed at about 33°C.

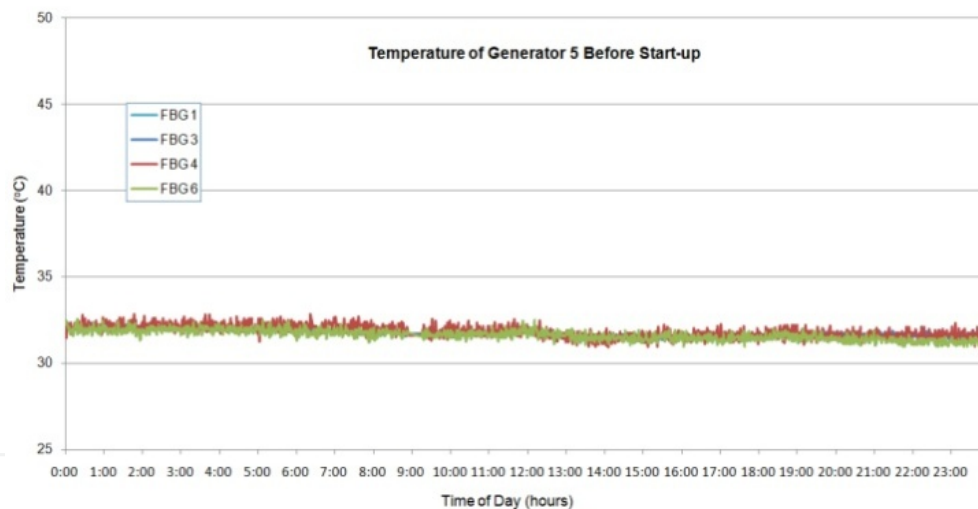


Figure 3. Temperature of generator 5 before start-up(adapted from [2]).

As part of the test procedures, the machine was started-up and shut down several times. The graph in Figure 4 shows the evolution of the temperature during the last start-up test of the generator. Notice that, in contrast to Figure 4, the temperatures of the radiators were not the same before the start-up. This is because previously the machine was working with different temperatures around the stator, which is normal, as we will see later. At 9 am the turbine was opened to the dam and the machine started-up. The temperature at FBG 3 rose from around 35°C to 85°C while the turbine accelerated to 90 rpm until in phase with the 60 Hz grid frequency. Then, at 6 pm the generator was switched to the national grid and the temperature rose again to 95°C, stabilizing thereafter.

Figure 5 shows the temperature of the generator when operating normally. At this time the generator was producing 22 MW with an average water flow of 82 m³/s.

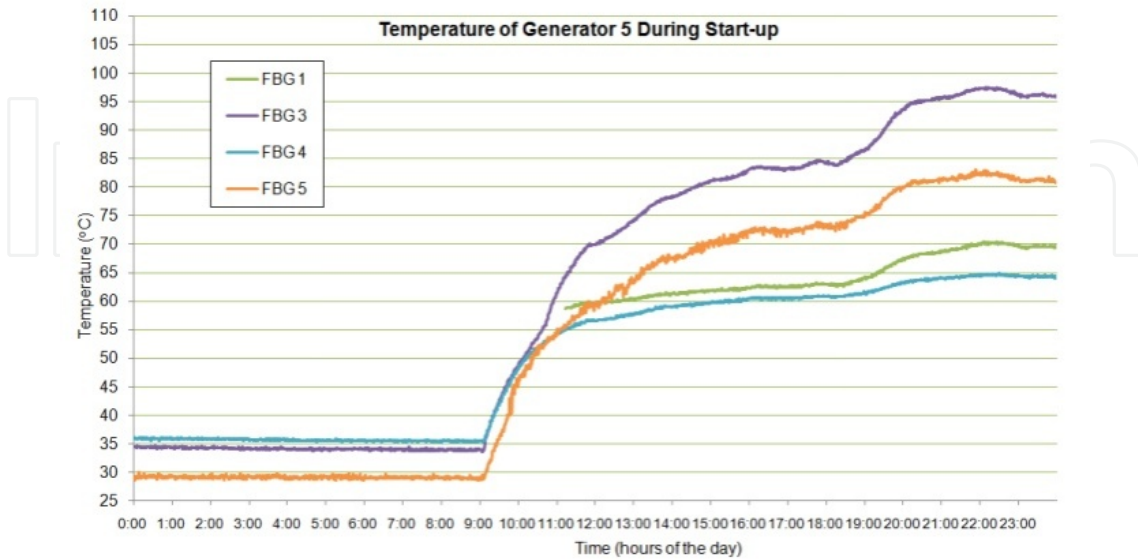


Figure 4. Temperature evolution of generator 5 during start-up(adapted from [2]).

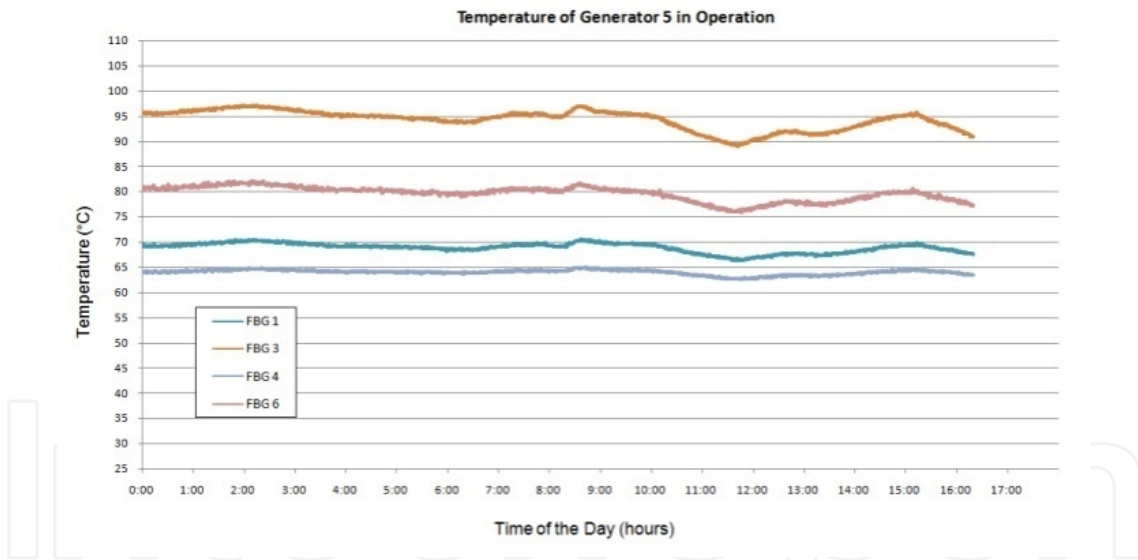


Figure 5. Temperature of generator 5 in operation (adapted from [2]).

It is worth pointing out that, in Figure 5 it is possible to see that, even in a steady state, the generator temperatures vary with time, with all temperatures following the same pattern. This is how the generator responds to the energy demands by the load.

As the final step of this project we needed to be sure that the temperature data monitored by our system was sufficiently accurate, after two years of operation inside the hydrogenerator. To accomplish this, we installed thermo-pair sensors which were physically attached to the FBGs copper tubing so as to compare conventional sensors with FBGs ones.

Thus we ended up with two sets of data for each radiator, one from our system itself and another one from the conventional thermo-pair datalog. Figure 6 shows the temperature evolution of one such measurements in which it is possible to see that both signals follow a similar pattern of behavior when the machine starts.

We can also observe that the thermo-pair sensor, being electronic and therefore subject to electromagnetic interference, produces a noisy output signal, differently from the FBG, which presents a smoother and asymptotic one, as expected.

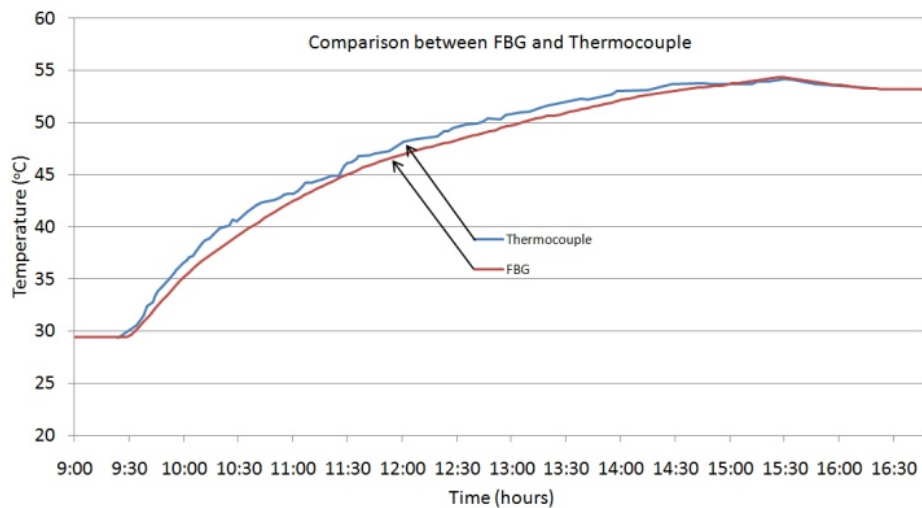


Figure 6. Comparison between an FBG sensor and a thermo-pair sensor as the machine starts (adapted from [2]).

1.4. Conclusions

This work describes the world's first application, test and operation of an FBG temperature sensor array inside a fully operational and connected-to-the-grid hydro-electric power generator.

A study of the sensing characteristics showed high repeatability, a maximum error of approximately 0.004°C (better than the calibrating thermometer) and linearity better than 99.9% for the five calibrated FBGs. These errors are related to the uncertainty of the interrogation system (± 1 pm) together with an FBG average sensitivity of about 13 pm/ $^{\circ}\text{C}$. Therefore, 1 pm in error means a temperature uncertainty of about 0.08°C . Since uncertainties below one degree centigrade are quite acceptable in the electric power industry, the calibration experiment demonstrated that the FBG system is appropriated for temperature measurements.

With this system in operation, a huge amount of installation and maintenance costs could be avoided with the replacement of many kilometers of electric wires by a few optical cables.

As a final conclusion, the system was capable of reliably and accurately measuring and monitoring temperatures inside the generator, even considering the harsh environment of the stator.

2. DC high voltage measurement based in an FBG-PZT sensor

2.1. Introduction

Electric power facilities, such as substations, rely on two basic instruments for their functionality and protection: the voltage transformer (VT) and the current transformer (CT) for measuring and controlling voltage and current, respectively. Those equipment are reliable for over-voltage and over-current protection, allow 0.2% revenue metering accuracy and their behaviour is well known both under normal and abnormal conditions. Nevertheless these equipments are made entirely of copper, ceramic and iron with all empty spaces filled with oil, which are weighty materials, producing bulky, heavy and clumsy equipment. On top of that, they tend to explode without prior warning, resulting in the potential destruction of nearby equipment by pieces of sharp ceramics and furthermore putting the substation personnel at risk.

Optical voltage transducers offer many improvements over traditional inductive and capacitive voltage transformers. These advantages include linear performance and wider dynamic range, not to mention, lighter weight, smaller size, and improved safety. Since optical fibers carry the measurements as light signal to and from the sensor head, workers and all substation control equipment are electrically isolated from the high voltage environment. Due to their small footprint and light weight, these pieces of equipment allow the maintenance of emergency mobile substations that are deployed on site by trucks and start working in a matter of a few hours. Optical CTs and VTs for power systems have been used in the last decades and are commercially available today from a few companies [3].

On the other hand, both Pockels and Faraday effects have drawbacks. The first one is that both Faraday and Pockels system components are not stable with temperature and stress, demanding the use of complicated compensation techniques [4] or specially designed optical fibers [5] in order to become reliable. Additionally, Pockels cells are made of bulk crystals, e.g. lithium niobate, demanding an open optics approach with lenses and polarizing filters which become an unstable and difficult-to-align system. The main drawback, however, is the high cost of this still new technology, not only for acquisition but also for maintenance, demanding specialty skills uncommonly available among company personnel.

From the demands of this work and the observations above, came the motivation for developing a practical VT system with two basic characteristics: a) intrinsic fiber optic sensors avoiding open optics and b) using a well-known and proven form of technology that would lead to a competitive price system as compared to conventional inductive VTs.

We have already designed and tested a hybrid electro-optical low cost monitoring system for the 13.8-kV distribution line [6], but nowadays the best technology for attending to the above demands is the fiber Bragg grating (FBG) that is relatively easy to deal with, reliable and very sensitive to strain. This section relates the development of a high voltage measuring system aimed to be used as the core of a 13.8-kV-class VT for the electric power industry application using as a sensing element a PZT crystal as voltage transducer and an FBG as strain measuring sensor.

2.2. Materials and methods

This section will develop the relationship between the resulted Bragg wavelength displacement when the optical fiber is submitted to a force applied by the PZT when the latter is subjected to an electric field.

As a first approach, the FBG was wound around a cylindrical PZT tube in a constant temperature environment as shown in the picture of Figure7.

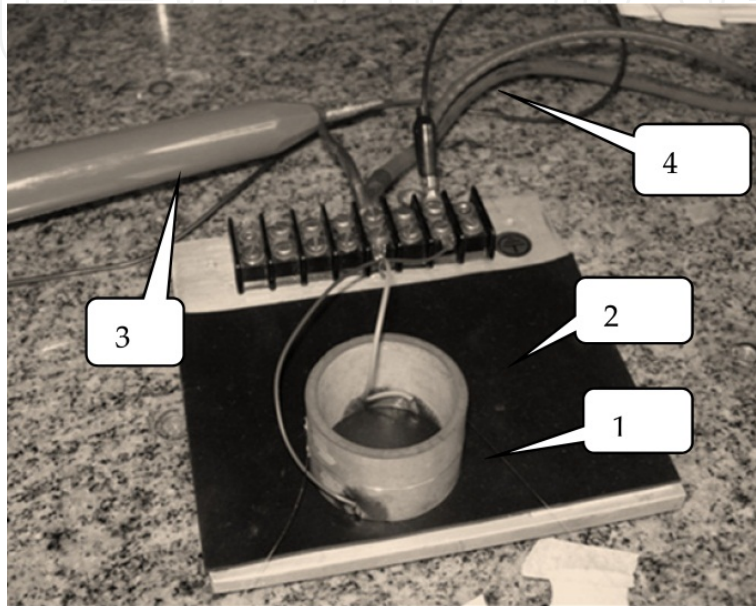


Figure 7. The optical fiber with a FBG (1) wound around the PZT crystal (2). Also shown are the high voltage probe (3) and the high voltage power supply leads (4).

When an electric field is applied to the PZT electrodes, the tube experiences both a circumference contraction (d_{31} is negative) and an increase in the wall thickness (d_{33} is positive). We can apply the following equation for calculating the net strain considering both effects.

For wall thickness displacement, we have:

$$\frac{\Delta w}{w} = d_{ij}E \quad (1)$$

where d_{ij} is the piezoelectric displacement coefficient (in meters per volt) with i being a designation for the direction crystal polarization and j being the Cartesian coordinate. The direction of polarization (axis 3) is established by a strong electrical field applied between the electrodes during the poling process.

Thus,

$$\Delta w = d_{33}Ew \quad (2)$$

But since the electrical field is

$$E = \frac{V_{in}}{w} \quad (3)$$

then we have:

$$\Delta w = d_{33} V_{in}. \quad (4)$$

Here V_{in} is the applied voltage and w is the wall thickness.

The cylinder wall thickness displacement will account for a variation of its diameter and consequently the length of the tube circumference, L , around which the fiber was wound.

Since $L=2\pi R$, we have $\Delta L=2\pi\Delta R$. Also, if the wall thickness is w , then, when the thickness increases by Δw , the radius R will increase by $\Delta w/2$, since half of the increase was in an inwards direction and does not account for ΔR . Then, we have:

$$\Delta L = 2\pi \frac{\Delta w}{2} = \pi\Delta w. \quad (5)$$

Substituting (4) into (5), we have the following fiber strain as a consequence of the wall thickness displacement:

$$\Delta L = \pi d_{33} V_{in} \quad (6)$$

But, as a result of the applied voltage, we also have a displacement of the circumference of the PZT tube. The relative increase of the circumference is, according to (2):

$$\frac{\Delta L}{L} = d_{31} E \quad (7)$$

or

$$\Delta L = 2\pi R d_{31} E \quad (8)$$

But, as $E=V_{in}/w$, we have:

$$\Delta L = 2\pi R d_{31} \frac{V_{in}}{w} \quad (9)$$

Finally, we add equations [6] and [9] to obtain the net effect:

$$\Delta L = V_{in} \left(\pi d_{33} + 2\pi R \frac{d_{31}}{w} \right) \quad (10)$$

or

$$\frac{\Delta L}{L} = V_{in} \left(\frac{d_{33}}{2R} + \frac{d_{31}}{w} \right) \quad (11)$$

For the PZT tube we have the following constants:

$d_{31}=-122$ pm/V; $d_{33}=300$ pm/V; $R=22.56 \times 10^{-3}$ m and $w=3.3 \times 10^{-3}$ m.

Substituting the above constants in (11) we have

$$\frac{\Delta L}{L} = -30.32 \times 10^{-9} V_{in}. \quad (12)$$

From Eq. (5) in [7] in a constant temperature environment and substituting the constants we have:

$$\frac{\Delta\lambda_B}{\lambda_B} = 0.78 \frac{\Delta L}{L} \quad (13)$$

Substituting (12) in (13) we finally have:

$$\frac{\Delta\lambda_B}{\lambda_B} = -23.65 \times 10^{-9} V_{in} \quad (14)$$

Now, considering the central Bragg wavelength at rest, $\lambda_B=1558.024$ nm, we get to the following sensitivity for our system:

$$\frac{\Delta\lambda_B}{\Delta V} = -36.85 \times 10^{-3} \text{ pm/V} \quad (15)$$

which means a Bragg wavelength shift of 36.85 pm per each 1000 V applied to the PZT.

In the next step, in order to increase the sensitivity, another approach was tested which is shown schematically in Figure 8. The PZT crystal was installed between the two levers and the fiber, with the FBG bonded on the levers' tips.

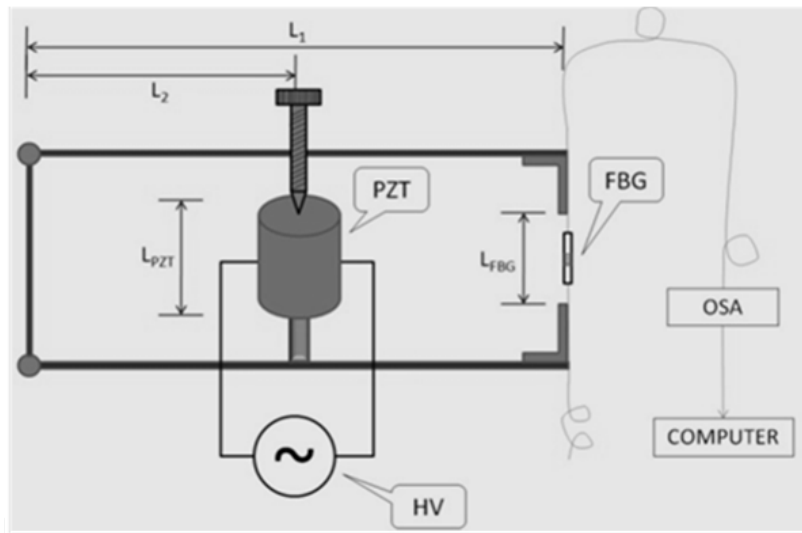


Figure 8. The setup with a variable-gain mechanical amplifier.

This setup consists of a mechanical amplifier with the possibility of varying the gain by changing the position of the tension screw along the upper lever.

The total gain G is, according to the parameters shown in Figure 8:

$$G = \frac{L_1}{L_2} \times \frac{L_{PZT}}{L_{FBG}} \quad (16)$$

This approach is based on the longitudinal mode strain of the PZT tube, that is, its length displacement. The position of the tension adjustment screw in the upper lever combined with the length of the PZT tube and the length of the optical fiber provided a mechanical strain amplification $G=1.98$.

We now have:

$$\frac{\Delta h}{h} = d_{32} \frac{V_{in}}{w} \quad (17)$$

Where $\frac{\Delta h}{h}$ is the relative change in height of the PZT tube, h is the height of the tube, w is the wall thickness and d_{32} is the piezoelectric coefficient in the longitudinal direction. These parameters have the following values: $h = 35 \text{ mm}$; $w = 3.3 \times 10^{-3} \text{ m}$ and $d_{32} = -122 \text{ pm/V}$.

Substituting the above constants in (17) we get:

$$\frac{\Delta h}{h} = -36.97 \times 10^{-9} V_{in}$$

But since we have a multiplication factor of 1.98, the strain experienced by the fiber will be

$$\frac{\Delta L}{L} = -73.20 \times 10^{-9} V_{in} \quad (18)$$

Now substituting (18) in (13) we have:

$$\frac{\Delta \lambda_B}{\lambda_B} = -57.10 \times 10^{-9} V_{in} \quad (19)$$

Considering a central Bragg wavelength at rest, $\lambda_B = 1560.025 \text{ nm}$, we arrive at the following sensitivity:

$$\frac{\Delta \lambda_B}{\Delta V} = -89.07 \times 10^{-3} \text{ pm/V} \quad (20)$$

which means a shift of 89.07 pm for each 1000 V applied to the PZT.

Figure 9 shows the complete setup with the Bragg meter and the high voltage power supply and Figure 10 shows a picture of the tube installed in the mechanical amplifier whose diagram was shown in Figure 7. The Bragg meter we used is the FS 2200 from Fiber Sensing, presenting a resolution of 1.0 pm and absolute accuracy of 2.0 pm.

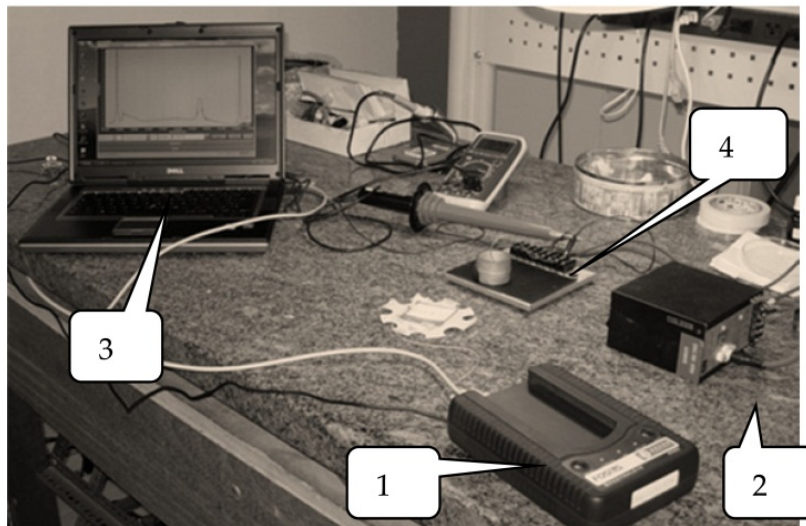


Figure 9. The complete setup showing the OSA (1), the high voltage power supply (2), the FBG spectrum (3) and the PZT crystal with the fiber wound around it (4).

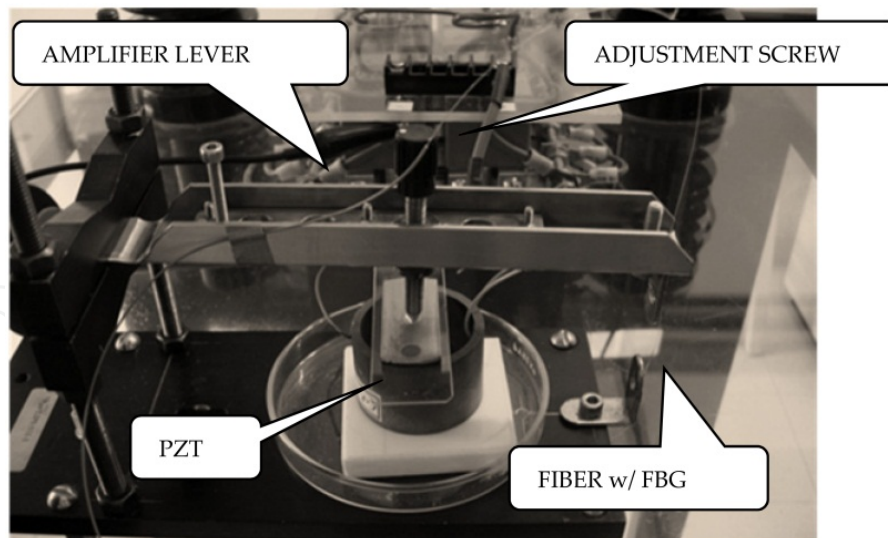


Figure 10. The PZT ceramic on the mechanical amplifier.

2.3. Results and discussions

For the first experiments, only DC voltages were applied to the PZT since the OSA we used to demodulate the FBG signal is too slow to respond to the 60Hz line frequency. The electro-optic setup was composed of an ASE light source, a 6 kV-DC variable power supply applied to the PZT, optical fibers inscribed with FBG and an OSA to trace the FBG's return signal and detect the center wavelength displacement.

In the first experiment the fiber was wound and glued around the PZT tube and for the second experiment the tube was fixed to the mechanical amplifier shown in Figure 10. This setup consists of a mechanical amplifier with the possibility of varying the gain by changing the position of the screw along the upper lever.

By applying a DC voltage to the PZT and recording the respective Bragg shift, it was possible to plot the graphs shown in Figure 11. The lower graph is the wavelength shift of the first experiment and the upper graph is the response of the second experiment. In this last experiment we used insulating oil in order to increase the applied voltage. The correlation coefficients (R^2) were 0.9936 and 0.9990 for the first and second experiment, respectively, which showed very good correlations and repeatability of the results in all measurements.

In the first experiment (fiber wound around PZT tube) the results obtained were shown by (15), or 36.85 pm per each 1000 V applied to the PZT. In this case we would have an inaccuracy of 13.6 V or about 1% of full scale. Obviously, this would not be satisfactory for a 0.2-class instrument transformer in revenue metering application.

In the second experiment (with mechanical amplifier) we obtained a wavelength shift of 89.07 pm for each 1000 V applied to the PZT (Equation (20)). Notice that in Figure 11 it is clear that there is a good relationship between wavelength and the applied voltage with a correlation coefficient of 0.9990. So the inaccuracy of this measurement could only come

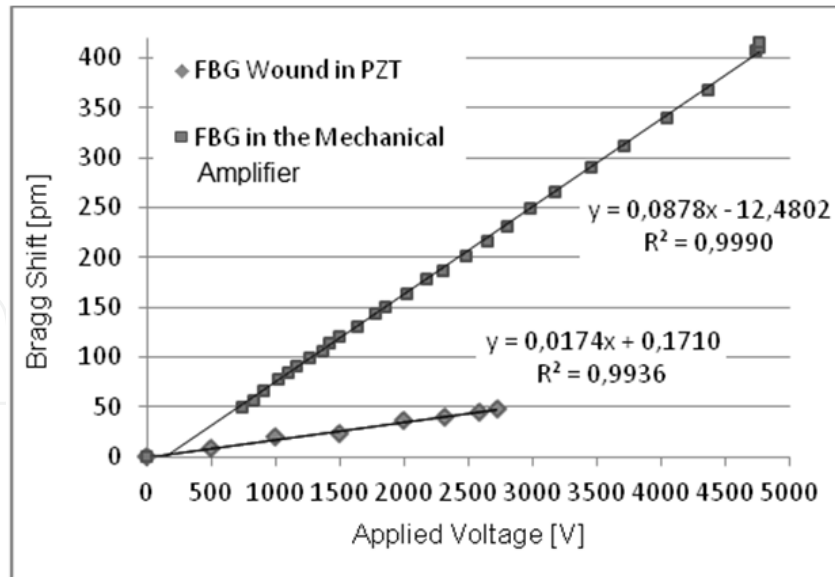


Figure 11. Bragg shift vs. applied voltage. The upper trace was obtained with the mechanical amplifier; the lower trace was obtained with the fiber wound around the PZT.

from the wavelength measurement by the Bragg Meter. Then, an inaccuracy in wavelength of 2.0 pm (the Bragg Meter's uncertainty) will lead to an inaccuracy in voltage of 22.45 V. In the TC's line voltage of 13.8 kV this error is 0.16%, meeting therefore the 0.2-Class of instrument transformer, IEC 60044-5 [8]. Since an increase in the gain (Eq. 16) leads to a larger sensitivity (Eq. 20) we can adjust the length L_2 in the amplifier and consequently decrease the error to a smaller value. Another alternative is to decrease the length of the FBG, L_{FBG} (Eq. 16) because this will also increase the gain.

2.4. Conclusions

The main conclusion of this work is that this setup can be used as a core of a practical 13.8 kV-Class VT if the issues mentioned above can be taken care off. Also, the difference from the maximum allowed voltage to be applied to PZT and the 13.8 kV expected to be measured can be easily circumvented by a capacitive divider. The divider will also be used when this system will be scalable to the 500kV-Class VT. These are preliminary results and a more appropriate setup is under development which will use the twin grating technique in order to demodulate AC voltages and a PZT disk stack to increase the longitudinal displacement and thus the fiber strain, resulting in an improved level of accuracy.

3. Measuring AC high voltage

3.1. Principle of operation of the FBG-PZT sensor

The experimental setup of the FBG-PZT sensor system is shown in Figure 12. The sensor was built by using a ceramic stack with ten 4-mm-thick PZT-4 rings, separated by 0.2-mm thick copper electrodes where the contacts were fixed. The proposed measurement system operates as follows: a voltage is applied in a combined PZT and FBG sensor by using a high

voltage power supply. This voltage acts on the PZT ceramic causing a mechanical deformation that is transmitted to an attached FBG used as interrogation system. Hence, the spectrum of the reflected light from the FBG is detected and demodulated to obtain a signal proportional to the applied voltage.

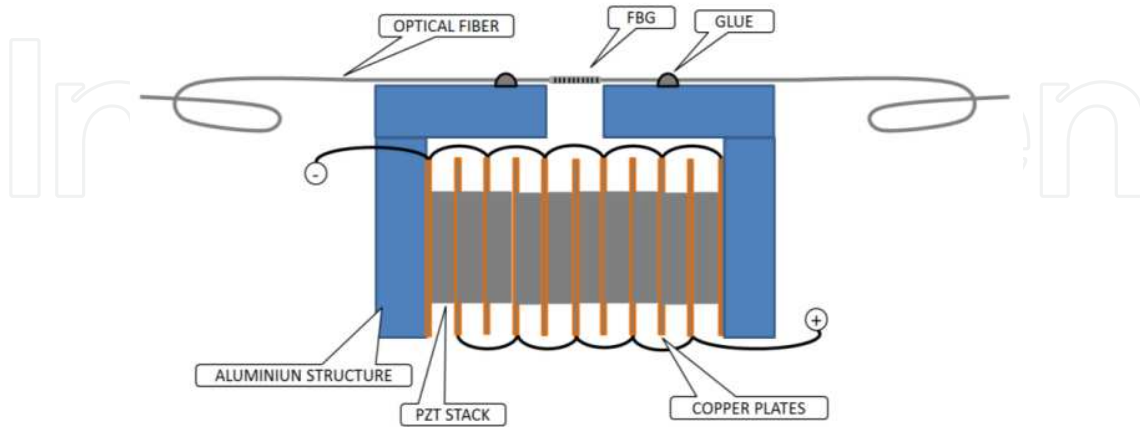


Figure 12. The mechanical setup comprised of ten ceramic disks in a stack. The polarization is made in such a way that all disks receive the same voltage [7].

The FBG with central wavelength of 1536.18 nm was stretched to 1538.48 nm before being bonded to the aluminum structure to allow measurements in both directions, since the PZT experiences positive and negative displacements when subjected to an AC voltage. For an improved isolation and to avoid sparks under higher voltages, the entire assembly was immersed in insulating oil.

For demodulating an FBG at DC operation one can use a commercial FBG interrogator as we can see in several low frequency applications. However, this equipment is limited to a few hertz, being incapable to respond to AC line frequency. We aimed the development of power line VT with an appropriated accuracy so as to attend the IEC [8] and also addressed to a study of temperature drift since temperature also displaces the Bragg wavelength, which is the measurement parameter. To calculate the sensitivity of the FBG-PZT transducer that is the relationship between the Bragg wavelength displacement and the electric field applied to the PZT we start from:

$$\frac{\Delta w}{w} = d_{33}E \quad (21)$$

Where w is the PZT disk thickness, $E=V/w$ and V is the applied voltage. Now, since the FBG is bonded to the side of the stack, it will experience the same strain as the PZT and we can combine Eq.(5) in [7] with (21) yielding:

$$\frac{\Delta \lambda_B}{\lambda_B} = (1 - \rho_e)d_{33} \frac{V}{w} + (\alpha + \eta)\Delta T \quad (22)$$

and for a constant temperature environment, we have:

$$\Delta \lambda_B = \lambda_B(1 - \rho_e)d_{33} \frac{V}{w} \quad (23)$$

Table 1 summarizes the parameters and constants for FBG and the PZT ceramic used in this work.

FBG	
Physical property	Value
Bragg wavelength (25°C)	$\lambda_B = 1538.48 \text{ nm}$
Photo-elastic coefficient	$\rho_e = 0.22$
Coefficient of thermal expansion	$\alpha = 0.55 \times 10^{-6}/^\circ\text{C}$
Thermo-optic coefficient (dn/dT)	$\eta = 8.6 \times 10^{-6}/^\circ\text{C}$
Length of fiber w/ FBG	$L = 28 \text{ mm}$
PZT	
Physical property	Value
PZT type	PZT4
Ceramic shape	Ring
Piezoelectric strain constant	$d_{33} = 300 \text{ pm/V}$
Thickness of ceramic	$w = 4 \text{ mm}$
Maximum direct field strength	1-2 kV/mm
Maximum reverse field strength	350-500 V/mm
Curie Temperature	$T_c = 325^\circ\text{C}$
Number of elements in stack	$n=10$

Table 1. PZT and FBG Parameters [7]

Substituting the PZT constants of Table I in (23) we have the following sensitivity:

$$\frac{\Delta\lambda_B}{\lambda_B} = 90.0 \text{ pm/kV} \quad (24)$$

which means a Bragg wavelength shift of 90 pm per each 1,000 V applied to the PZT. If we want to comply with the IEC 60044-5 [8] when measuring 13.8 kV, a conventional class for distribution line, we must attain 0.2% accuracy and so be capable to distinguish accurately at least 27.6 V when measuring the applied voltage using the wavelength displacement. According to (24), 27.6 V is equivalent to a Bragg shift of 2.48 pm which is very close to the accuracy of Bragg Meters commercially available (approximately ± 2.0 pm). Clearly, the final accuracy does not depend only on the measuring capacity of the Bragg Meter, as many other factors interfere, but the Bragg Meter's accuracy imposes a lower limit.

Werneck et al [6] have used a mechanical amplifier in order to multiply the strain and obtain a larger amount of Bragg displacement, that is, a higher sensitivity. The authors used a stack made up of ten PZT rings in a parallel polarization scheme. Also, by decreasing the fiber length in the mechanical setup increases the FBG strain, as will be seen in the sequence.

For calculating the sensitivity of this setup we rewrite (21) including n , the number of PZT elements:

$$\Delta w = n d_{33} V \quad (25)$$

Since the FBG is bonded between the two fixing points of the stack, the displacement previewed by (25) will be transmitted to the fiber, so that

$$\Delta w = \Delta L_{\text{FBG}} \quad (26)$$

Now combining Eq. (5) in [7], (25) and (26), and considering $\Delta T=0$ (constant temperature environment), we get to:

$$\Delta\lambda_B = \lambda_B(1 - \rho_e) \frac{nd_{33}V}{L_{\text{FBG}}} \quad (27)$$

Substituting the PZT constants in (27) we have the following sensitivity:

$$\frac{\Delta\lambda_B}{\Delta V} = 128.6 \text{ pm/kV} \quad (28)$$

3.2. Optical setup for DC input

The block diagram of the optical setup for DC input is shown in Figure 13. A variable high voltage DC power supply was used to test the system. An ASE (Amplified Spontaneous Emission) broadband light source illuminates the FBG and its reflected peak is directed to an optical spectrum analyzer (OSA) which is controlled and monitored by a computer, the dotted-line box in Figure 13 encompasses the commercial optical interrogator with a resolution of 2.0 pm. With this setup it is possible to read the wavelength displacement of the sensor and relate it with the DC input voltage applied using a high voltage source. Using this scheme it is possible to test and calibrate the system.

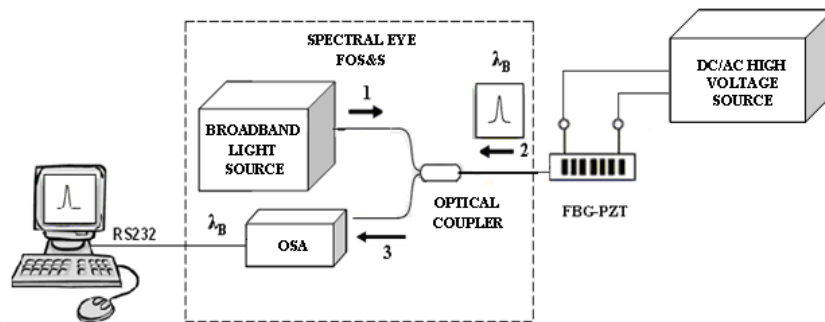


Figure 13. Schematic diagram of the setup for DC input.

3.3. Optical setup for AC input

As mentioned before, commercial OSAs are too slow to respond to the 60-Hz line frequency. For AC voltage measurements we used the interrogation system shown in Figure 14. A high voltage AC source was used to supply the input signal to the PZT electrodes. A broadband light source was used to illuminate the FBG-PZT sensor via an optical circulator. The reflected spectrum of the sensor passes through a Fabry-Perot (FP) tunable filter with a 0.89 nm bandwidth. The resulted signal at the output of the FP filter is the convolution between the reflected FBG spectrum and the FP transmission spectrum. The optimum position of the center wavelength of the FP filter is chosen by a novel algorithm developed

by [9]. The dashed area on the spectrum drawing at the left of the FP filter in Figure 14 is the intersection between the spectrum of the reflected signal and the band pass of the FP filter. The integral of this area is the total light power that exits the filter and reaches the photodetector. The intersection point of the two spectra occurs at the linear portion of each curve, therefore when the sensor spectrum moves, the superimposed area varies linearly.

Since the sensor spectrum is oscillating at 60 Hz, the intersection will increase and decrease accordingly and the output power of the filter will also oscillate at the same frequency. After this demodulation process, the amplitude (power) of the light signal is proportional to the instantaneous input voltage applied to the PZT. The signal is then fed into an amplified photodetector which output voltage signal is analyzed by an oscilloscope.

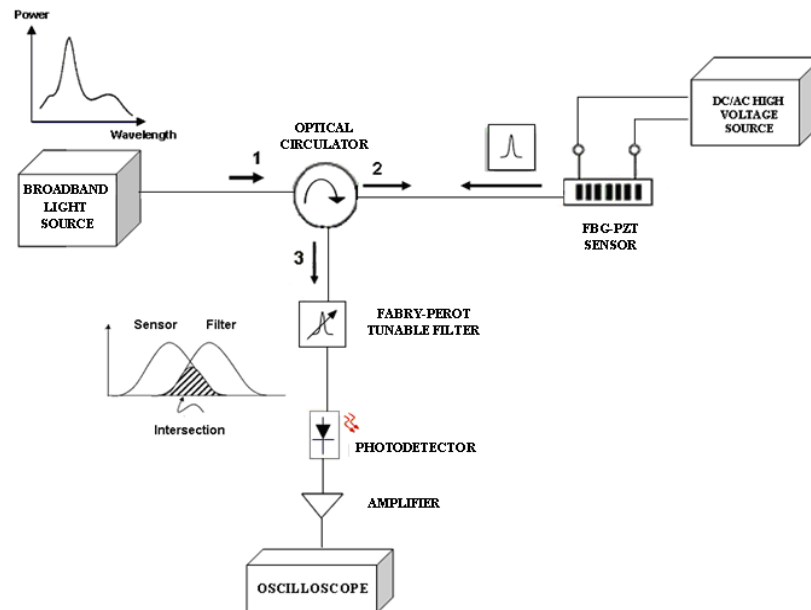


Figure 14. Schematic diagram of the setup for AC voltage using a tunable Fabry-Perot filter.

3.4. Results and discussion

For the first experiment, DC voltages were applied to the FBG-PZT to measure the Bragg displacement by the interrogation system shown in Figure 13. The applied voltage to the PZT ranged from 0 V to 2250 V approximately to not exceed the maximum electric field in direct and reverse directions, specified by the ceramic datasheet. By applying a DC voltage to the PZT and recording the respective Bragg shift, it was possible to plot the graphs shown in Figure 15.

For multiple measurements, we found the average linear sensitivity of 89.09 pm/kV for the FBG-PZT sensor and an average correlation coefficient of $R^2=0.9985$. The recorded sensitivity indicated a Bragg wavelength shift of 89.09 pm per 1000 V applied to the terminals of the PZT.

The voltage dependent sensitivity was calculated and Figure 15 shows the results for 10 measurements. By using a linear fitting procedure (Matlab) the uncertainty studies regarding these results indicate an RMSE of 0.0025 kV and an average standard deviation of 1.19 pm

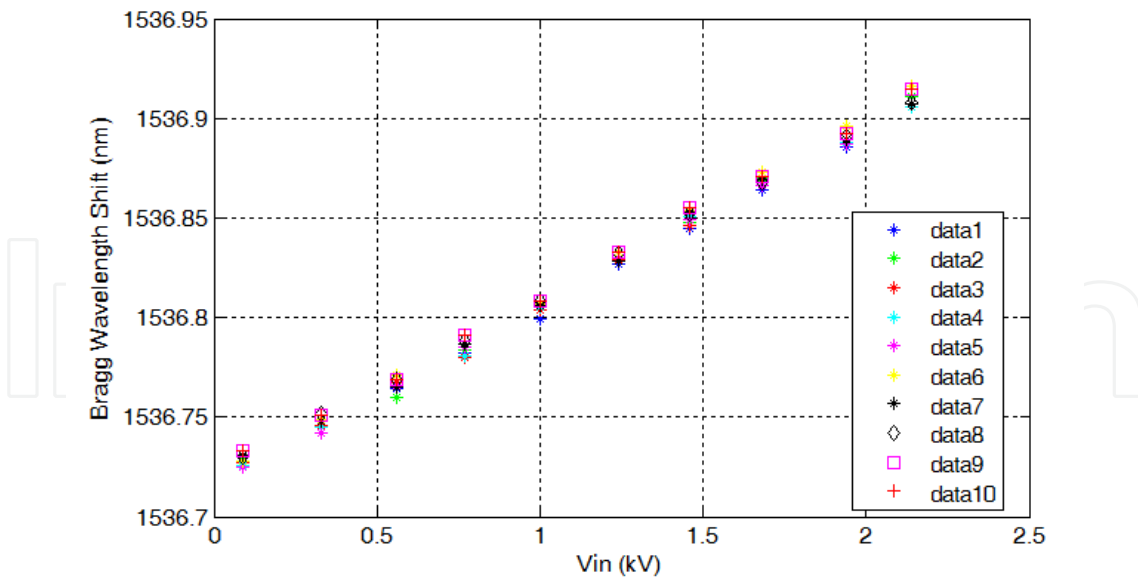


Figure 15. Relationship between the DC voltage applied to FBG-PZT and the Bragg wavelength shift.

which, when divided by the sensitivity, produces an uncertainty in voltage measurement of 13.36 V. This error in voltage represents an uncertainty of 0.09 % in the 13.8 kV Class, which is very close to the 0.2% accuracy needed to comply with the IEC for DC measurements. According to the transducer errors on Figure16, the maximum and minimum residual errors were 0.005 kV and 0.007 kV when measuring0.09 kV and 0.56 kV respectively. This dispersion presented on the results was due to inaccuracies of the system, as well as OSA uncertainty.

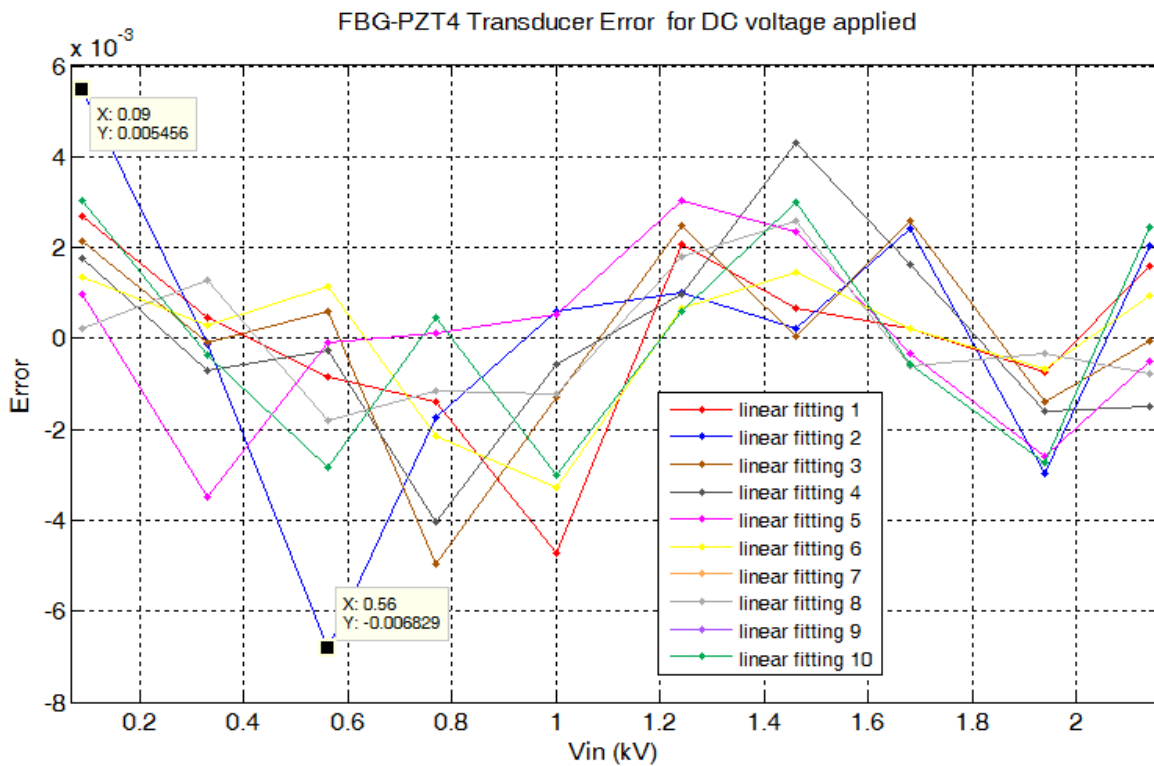


Figure 16. The FBG-PZT transducer errors for DC voltage applied.

The obtained average experimental sensitivity of 89.09 pm/kV for FBG-PZT sensor was smaller than that expected by the theoretical analysis shown in (28): 128.6 pm/kV. The reason for this difference may be related to the elasticity of the materials employed in the mechanical setup. When a voltage is applied to the PZT that forces its displacement, the optical fiber bonded to the aluminum assembly pulls in the opposite direction. If the structure relaxes, the fiber will not be completely stretched, thus preventing full displacement.

The Young's modulus of the optical fiber (70 GPa) is of the same order of magnitude as that of aluminum (69 GPa); however, this cannot be attributed to the aluminum stretching, because its cross section area is much larger than that of the fiber. However, the adhesive used to bond the stack together is fairly elastic, and might easily relax by a few nanometers, which is enough to lower the fiber displacement, resulting in lower sensitivity as the fiber is stressed less than that theoretically calculated.

The AC measurement results consist of measuring the variations in the Bragg wavelength, converted from the photodetector output voltage as a function of AC voltage applied to the terminals of the FBG sensor FBG-PZT. By applying an AC voltage to the PZT and measuring the output voltage of the amplifier over six consecutive cycles, it was possible to obtain the plots shown in Figure 17. The sensor response to an applied voltage in the range of 0 kV to 2 kV, approximately, is presented. A linear relation was found with an average sensitivity of 0.087 and an average correlation coefficient of R^2 0.9983.

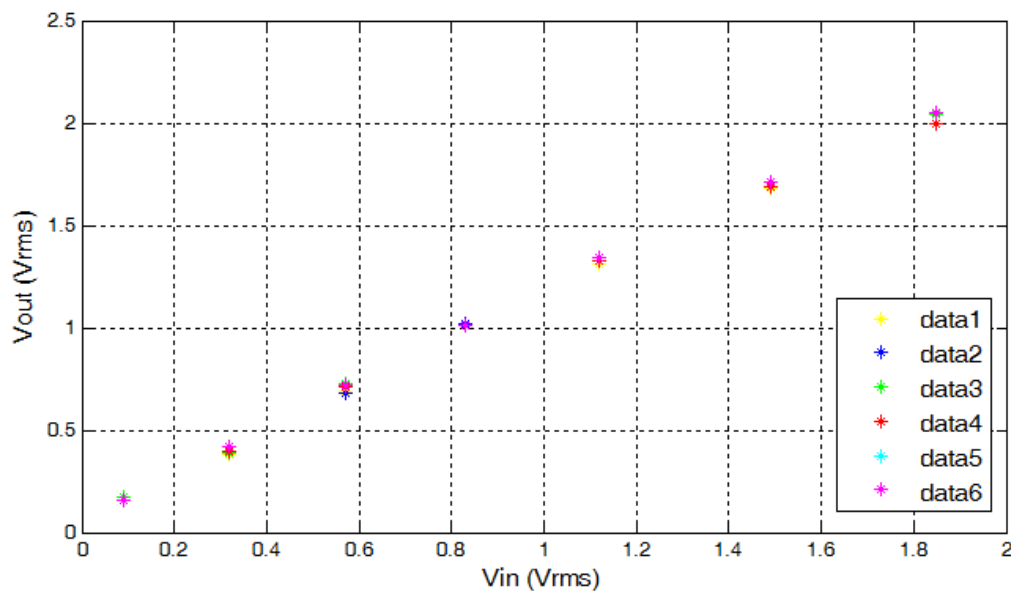


Figure 17. Relationship between the input and output voltages using the Fabry-Perot filter.

Figure 18 shows the linear fitting results for six measurements. According to Figure 18, one can conclude that the maximum error was 0.05 kV on 0.83 kV and the average RMSE was 0.0314 kV.

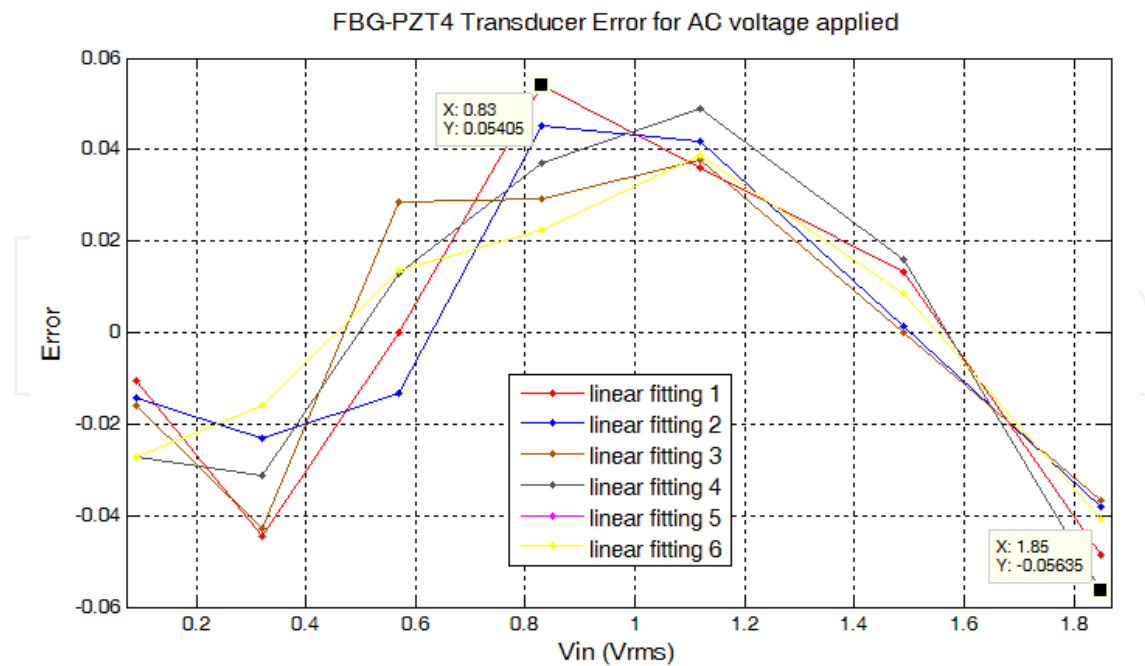


Figure 18. The FBG-PZT transducer errors for AC voltage applied.

For the analysis of dynamic measurements of the output signal it is necessary to measure the total harmonic distortion (THD) of the input signal. Figure 19 shows the wave form of the signal from the measurement system. The objective of this analysis was to investigate the behavior of the input signal (60 Hz line signal) and measure the output harmonic distortion, as the applied AC voltage is increased. The obtained THD was 4.72% and this low value ensures that the harmonic distortion in AC results is not related to the input signal. We can notice that the measurement system output THD occurs particularly when the input voltage reaches the end of the scale, approximately at 1700 V. The reason for this harmonic distortion is that the input signal reaches a nonlinear region of the convolution function between FBG and FP filter spectra. A photograph of the experimental setup can be seen in Figure 20.

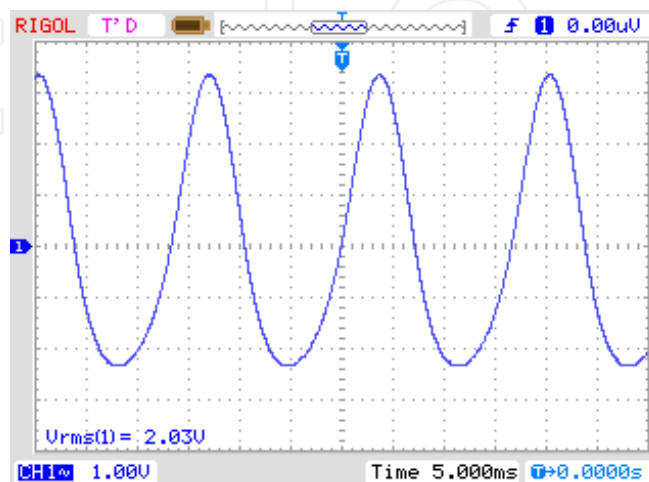


Figure 19. Photodetector output signal for increment of the applied AC voltage (Vrms).



Figure 20. Experiment Setup for AC/DC measurements.

3.5. Temperature drift study

Equation (5) in [7] shows that the temperature also displaces the central wavelength of an FBG. This is because α , the thermal expansion coefficient of the silica, and η , the thermo-optic coefficient, are temperature dependent parameters. However, if the FBG is bonded to an aluminum assembly, the Bragg wavelength will drift with temperature, not only due to α and η but also due to the thermal expansion coefficient of the aluminum. Now, if the sensor center wavelength drifts, its gain and sensitivity will vary accordingly.

There are four options to circumvent this effect. The first option is to measure the PZT temperature by using another FBG, and calculating the respective Bragg drift. Hence, an automated controller could adjust the FP filter accordingly. The second option, which only works with twin FBGs, is simply performed by placing the FBG-filter into the same thermal environment as the PZT. In this way, both FBGs will drift together, and the optimum position will be maintained.

The third option requires an engineered assembly so that the thermal expansion is compensated by counter balanced strains. If the PZT stack presented the same strain as the strain of the aluminum ends of the assembly, the fiber and the FBG would not be subject to any strain because the stack displacement would be counterbalanced by the supporting ends. Since the thermal expansion coefficient of aluminum ($24 \times 10^{-6}/^{\circ}\text{C}$) is greater than that of the PZT4 ($4.5 \times 10^{-6}/^{\circ}\text{C}$), we would need a stack length greater than that of the supporting ends to have a counterbalancing effect. Of course, we would also have to include the thermal expansion of the optical fiber ($0.55 \times 10^{-6}/^{\circ}\text{C}$) for the perfect match.

To check this approach the sensor was inserted inside an oven from 25°C to 45°C , without any voltage applied to the PZT4. Figure 21 shows a linear Bragg wavelength displacement with a negative slope as the temperature is varied. The negative slope indicates that the fiber was relaxed instead of being pulled by thermal displacement. The linear fitting for this

measurement shows a response for the temperature sensitivity of 55.11 pm/°C with a maximum error of 0.03 kV on 45°C.

In reality, since the thermal coefficient ratio between aluminum and PZT is 5.33, to obtain a perfect match, the total length of aluminum parts should be 5.33 times smaller than that of the PZT stack, which would compromise the project. However a few other materials are available, such as titanium, which has a thermal expansion of $8.6 \times 10^{-6}/^\circ\text{C}$. In this case, the ratio of titanium parts over PZT parts would be around 2, which is reasonable.

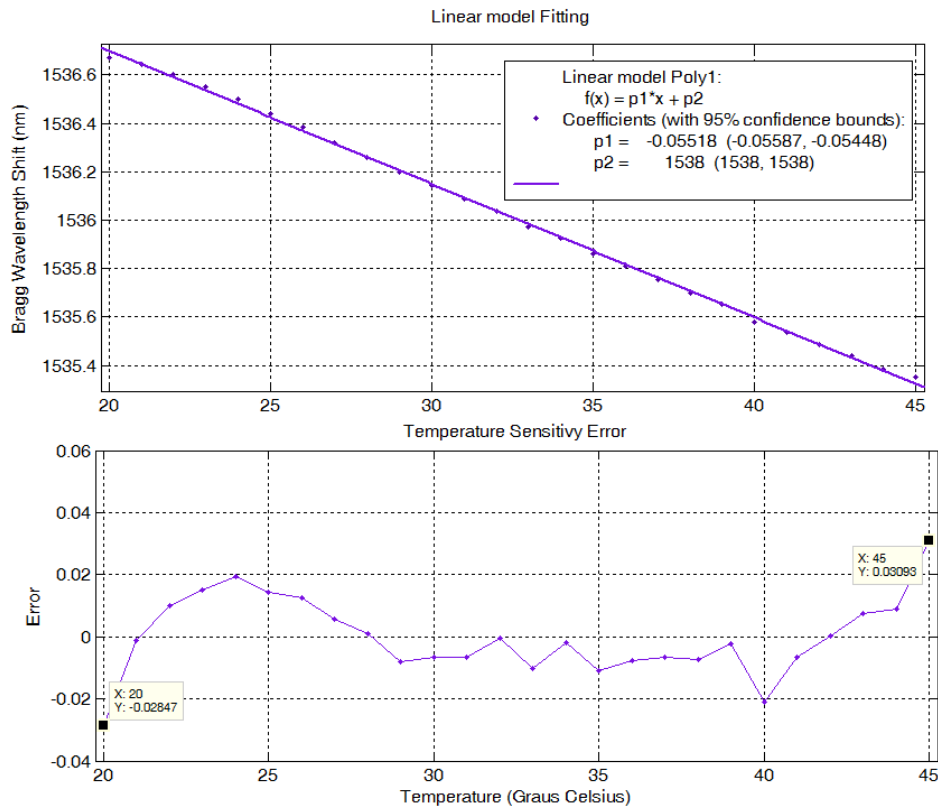


Figure 21. Thermal sensitivity of the FBG-PZT sensor.

3.6. Conclusions

A new optical voltage transformer (OVT) measurement scheme for an AC high voltage line was developed, bearing in mind accuracy, repeatability, and reliability, and was appropriated to in-field operation, and able to comply with the standard IEC 60044-5 [8]. This setup may be used as the core of a practical 13.8 kV-Class VT, as long as temperature compensation is addressed appropriately. As for a possible commercial production of OVTs using the techniques proposed here, it is worth recalling that in recent years the extensive development of optical devices for the telecommunications market has improved their reliability, and, at the same time, decreased their cost. In addition, the devices used in our prototypes, such as PZT crystals, FBG sensors, broadband light source, and an amplified In GaAs photodetector, are not more expensive than the components used in conventional VTs. For this reason, it is considered that the final fabrication costs would not exceed those of conventional VTs.

4. Measuring current in HV transmission lines

4.1. Hybrid devices and magnetostriction

Consistent current measurements are obligatory in several situations, such as in substations, power transmission and oil industry [10, 11]. Usually instrument transformers in electric power facilities are massive and heavy equipment. In this sense, numerous current sensing schemes which make use of the Faraday Effect have been proposed, since optical systems frequently offer a wider dynamic range, lighter weight, improved safety and electromagnetic interference immunity [12].

Several indoor designs of hybrid optical current sensors have been presented, some of which explore the magnetostrictive actuation of a ferromagnetic rod over a fiber Bragg grating, which is attached to this material. All magnetic materials present the magnetostrictive phenomenon, in which the material suffers a strain due to the application of a magnetic field, i. e, the magnetic sample shrinks (negative magnetostriction) or expands (positive magnetostriction) in the direction of magnetization [13]. Thus, magnetostrictive materials (MM) convert magnetic energy into mechanical energy, and the inverse is also true, i.e., when the material suffers an external induced strain its magnetic state is altered. A typical length variation curve showed by this kind of material is presented in Figure 22 [14], where in region 3 the saturation state has been reached ($\Delta L/L$ is the strain). The FBG is frequently attached to the material using a common adhesive, usually cyanoacrylate glue. Thus, as the magnetostrictive rod is strained by the application of a magnetic field (generated, for instance, by an electrical current), also it is the grating, providing a current measurement that is wavelength encoded. This sensor head arrangement is presented in Figure 23.

In [15] the first studies concerning the use of FBGs and MM in DC electrical current measurements are described. In this proposed system two different alloys are employed as the sensor head, being one of them a magnetostrictive rod and both with the same thermal expansion coefficient. In each alloy there is an attached FBG, written in the same optical path. While the Terfenol-D (which is a rare-earth magnetostrictive alloy) rod is used to

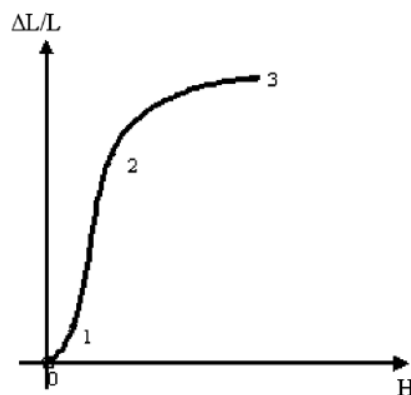


Figure 22. Magnetostrictive material strain characteristic [14].

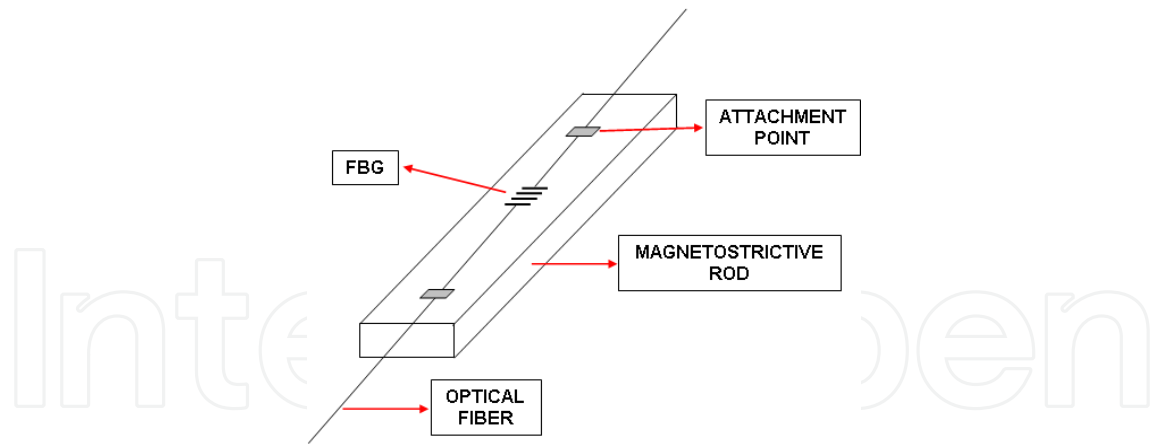


Figure 23. FBG attachment arrangement (sensor head).

obtain the current measurement itself, as it strains the FBG, the grating attached to the non-magnetic alloy provides data concerning temperature variations, acting as a reference for thermal compensations. In this way, when there is a temperature variation both gratings are subjected to the same thermal expansion, the difference between the Bragg wavelengths is a measure of the magnetostriction, and the FBG attached to the non-magnetic alloy (MONEL 400 – a nickel, copper and iron alloy) provides information about the temperature. This sensor head schematic is showed in Figure 24.

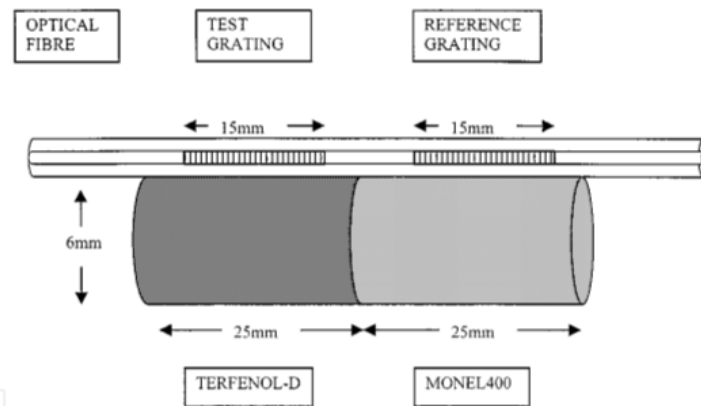


Figure 24. Sensor head for DC-current and temperature measurement [15].

The several advantages showed by the FBG sensing technology in high voltage environments have boosted the development of a number of current measurement systems, especially for the power industry. An optical current transformer (OCT) based on Terfenol-D actuation for AC current signals is proposed in [16], where a prototype to be used in a 100 – 1000 A measurement range was constructed. A testing matrix was made in order to investigate an optimized sensor head operating point, in terms of mechanic and magnetic biases. Since magnetostriction is a unipolar phenomenon, i.e., its output is rectified, to obtain a bipolar response the system must operate in its liner region (region between 1 and 2 in Figure 22) by the application of a DC biasing magnetic field (Figure 25a). This matrix consisted in a C yoke that was turned into a closed loop, the sensor is located in the forth arm (Figure 25b).

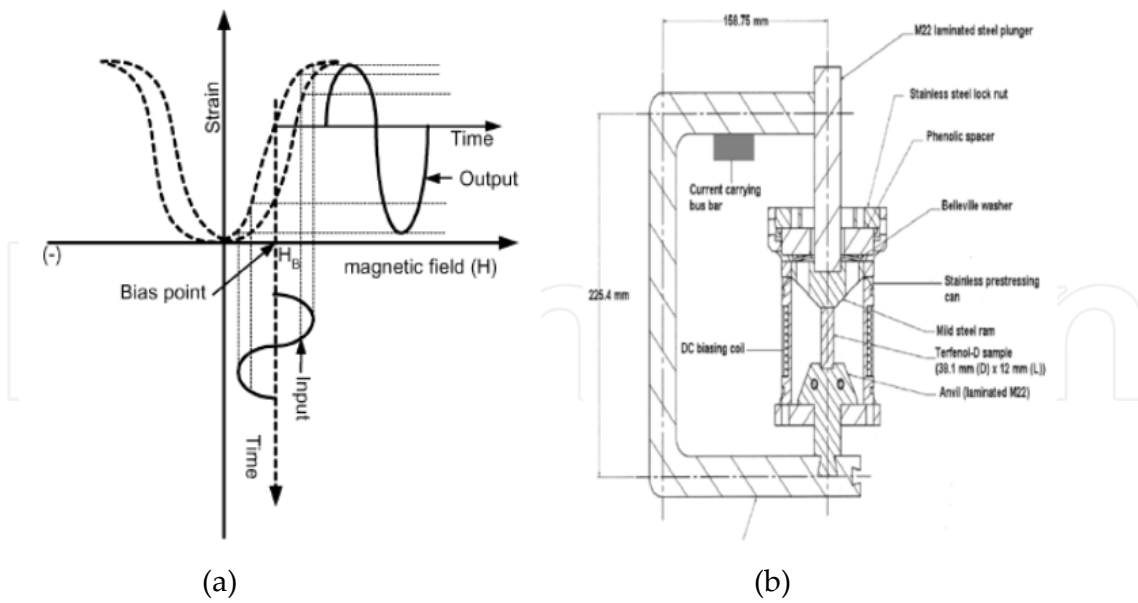


Figure 25. (a) A biasing field which allows the measurement of AC signals, (b) Test matrix for system optimization [16].

A monitoring system specifically proposed for transmission lines (TL) is proposed in [17]. In this particular case a different sensor head arrangement is discussed – a coil is not used to excite the optical-magnetostrictive measurement set-up – instead, a uniform FBG with Bragg wavelength of 1531.56 nm is fixed to a magnetostrictive rod, which is positioned at a distance D from the center of the transmission line conductor cable (Figure 26) and parallel to the direction of the current generated magnetic field lines. In this proposal, temperature and TL ac-current can theoretically be measured, where the current is amplitude codified and the temperature is wavelength codified, so there is no ambiguity. The sensor head can be operated at long distances (approximately 2 km) and since an optical fiber path is being employed there is an intrinsic multiplexing capability; however, optical attenuations must be accounted for.

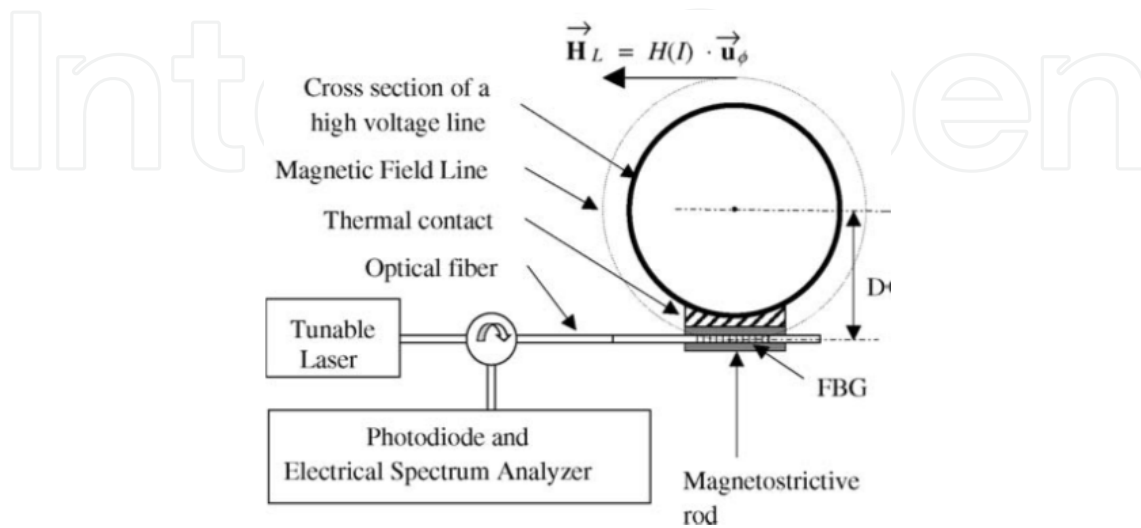


Figure 26. High voltage line sensor head, proposed in [17].

But the usual proposed demodulation techniques are still expensive or not suitable for a prolonged in-field operation. In this section, two opto-mechanical sensor head are showed and compared as current transducers. A laboratory test device for nickel and Terfenol-D is showed, the designed transducers were tested and the temperature effect on the measurement responses was evaluated for a more accurate estimate of the transducers response range.

4.2. Materials and methods

Two transducer configurations are investigated. The main difference lies in the employed materials; nickel and Terfenol-D are utilized as the main parts of the transducer systems. When submitted to a magnetic field generated by the electrical current to be measured, the nickel rod longitudinal length is reduced, while in Terfenol-D the opposite effect occurs, i.e., the material elongates. In this sense, the magnetostrictive samples treatment procedure and the developed electrical current source used to excite the sensor heads are described.

Untreated nickel samples, with dimensions of 100 mm X 100 mm X 10 mm, to be used as magnetic-mechanical transducers need to go through a hot rolling procedure. This method provides thin nickel sheets, thus allowing the reduction of eddy currents. A piece of raw nickel was heated in a metallurgical furnace at a temperature of 600°C for a 10-minute period. After that, the nickel piece is removed from the oven and submitted to metalworking. This procedure was repeated five times, until the nickel sheet reached the thickness of 0.5 mm. This sheet was cut into smaller pieces, with dimensions of 100 mm X 10mm X 0.5 mm, and piled up in a number of seven, which were glued together with an insulating varnish, composing a complete magnetostrictive part with approximate dimensions of 100 mm X 10 mm X 3.5 mm. This arrangement, besides reducing the effect of eddy currents, is a more robust scheme.

A Terfenol-D rod, an alloy composed by iron, terbium and dysprosium (a Giant Magnetostrictive Material – GMM) with dimensions of 80 mm X 10 mm X 10mm) was used. The material is solid and brittle (Figure 27).

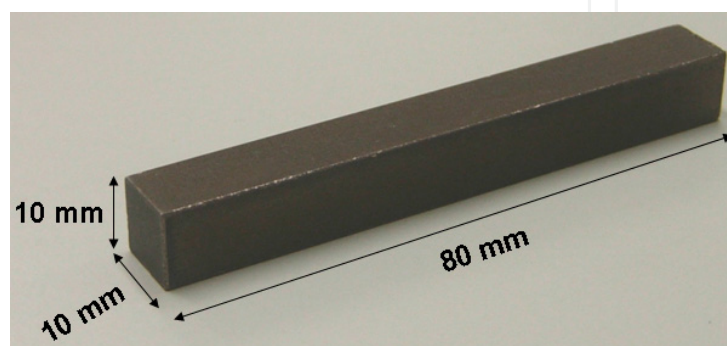


Figure 27. Terfenol-D rod.

Two fiber Bragg gratings were fixed to the MM using commercial cyanoacrylate adhesive, after the cleaning of both nickel and Terfenol-D surfaces, this procedure enables an improved attachment. The FBGs are also stretched, a procedure which will allow the monitoring of magneto-elastic elongations and compressions that the materials may suffer when submitted to magnetic fields. A stretching device is employed in the fibers stretching procedure; while an FBG interrogator was used to monitor the Bragg wavelength shift (Figure 28).

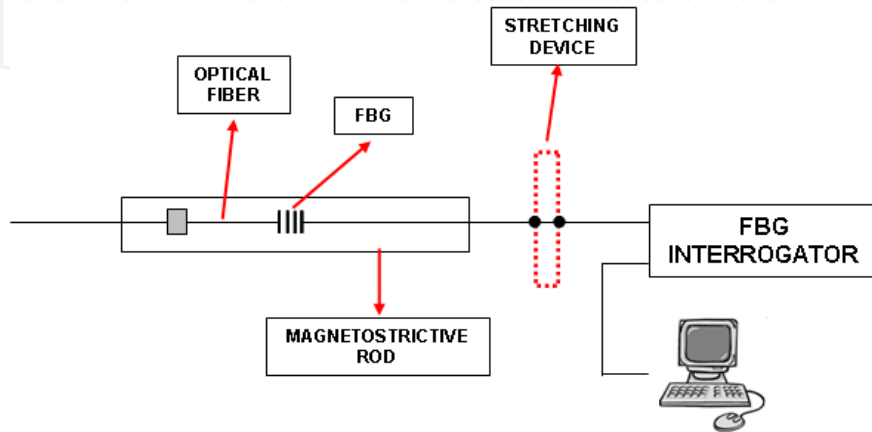


Figure 28. FBG stretching scheme, prior to complete attachment

In order to investigate the magnetostrictive characteristics of both nickel and Terfenol-D samples and to study the proper attachment of both gratings over these rods, a coil was constructed, enabling the excitation of the opto-mechanical transducers with DC current, thus DC magnetic fields. Therefore, the testing system consists in a driving circuit and an exciting coil, fed with DC electrical currents, hence providing a scheme for the magnetostrictive activation.

4.3. Experiments

The transducer devices are positioned in the core of the exciting coil (Figure 29), which is mechanically supported by a PVC tube. Considering this arrangement, a current range of 0 – 27 A_{DC} was delivered to the load, while the Bragg wavelength shift and the transducers temperature were monitored. It is important to monitor the temperature to which the sensor heads are submitted, since there is power dissipation as the DC current is developed in the coil, thus increasing the sensor head temperature. The maximum current was limited by the variable transformer capacity.

The first transducer to be investigated was the one prepared with the stacked nickel sheets, composing a rod. A fiber Bragg grating with $\lambda_B=1538.176$ nm at 25°C was attached to the rod, and therefore exposed to the magnetic field generated by the current in the exciting coil. Four measurement cycles were carried out, and the obtained curves are presented in Figure 30. A tendency line that adjusts the data and its equation, the theoretical values of the magnetic field and the temperature of the rod during the experiment, are also presented.



Figure 29. Assembled activation coil, designed according to the procedure described in [18]

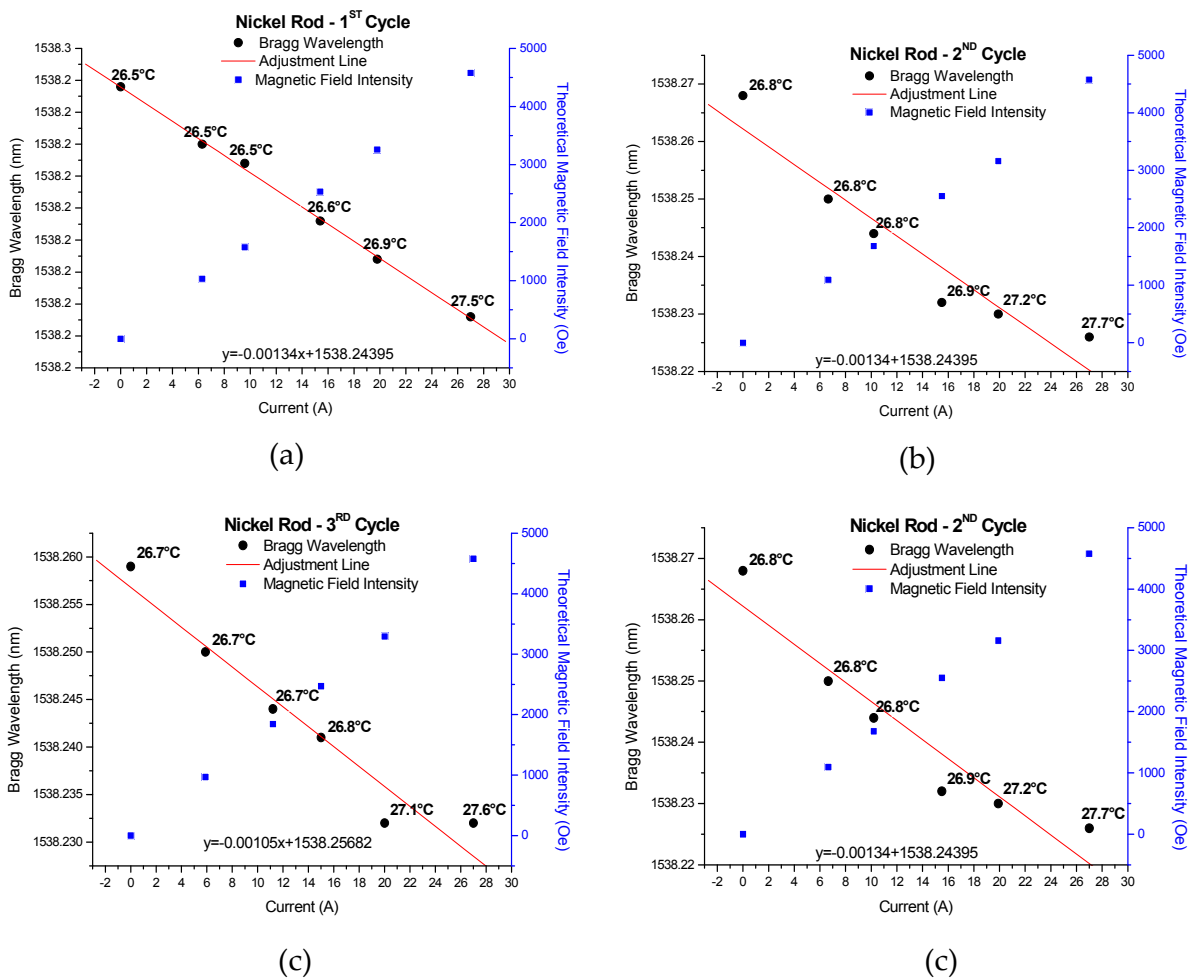


Figure 30. Bragg wavelength λ electrical current curves for the FBG-nickel-based sensor head, for four measurement cycles.

The Terfenol-D-based sensor head was also studied. In this case, an FBG with $\lambda_B=1540.065$ nm at 25°C was fixed on the alloy rod. Repeating the previously described testing procedure, the obtained Bragg wavelength X electrical current curve is showed in Figure 31. A tendency line that adjusts the data, the theoretical values of the magnetic field, and the temperature of the rod during the experiment, are also presented.

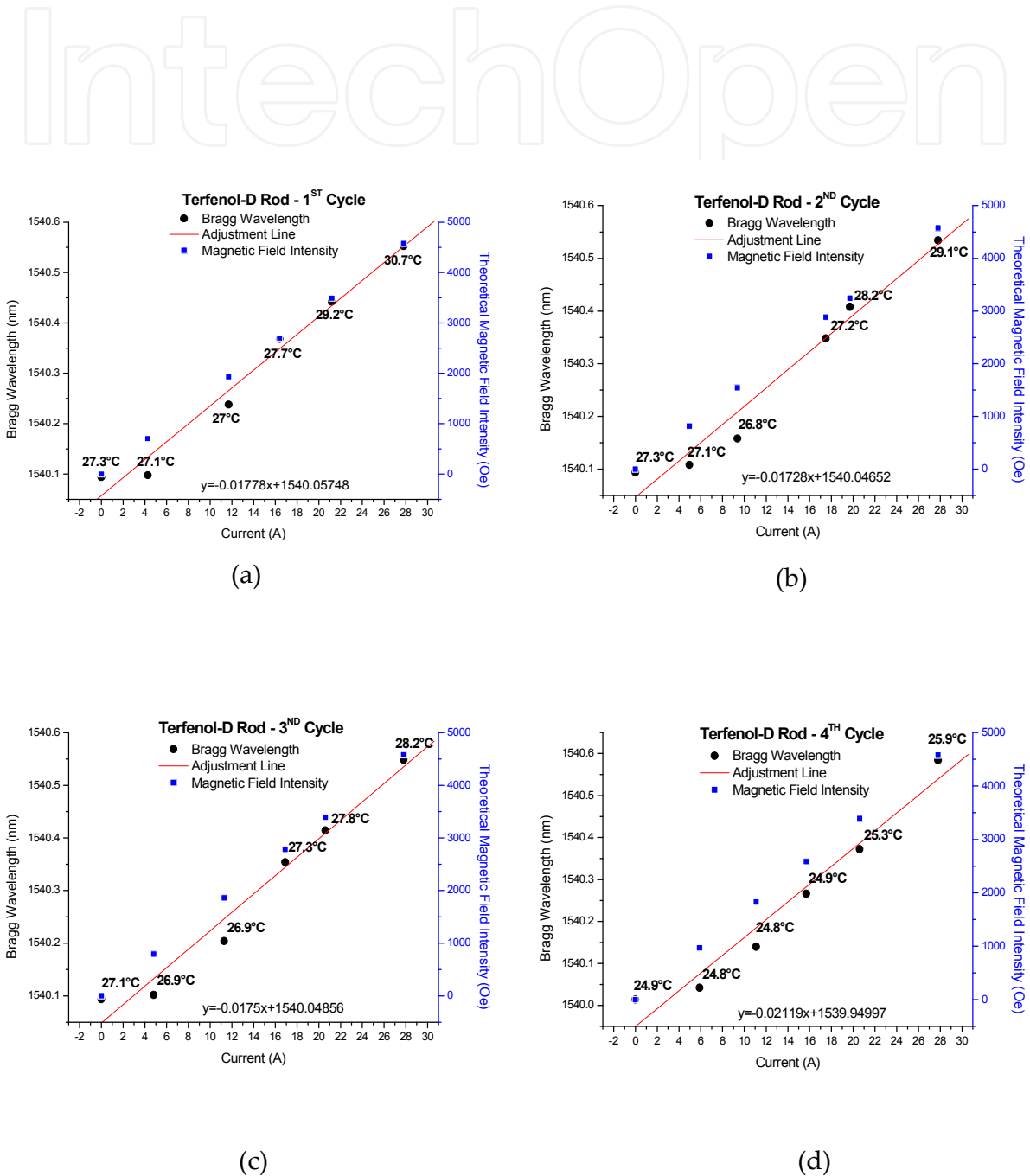


Figure 31. Bragg wavelength X electrical current curves for the FBG-Terfenol-D-based sensor head, for four measurement cycles

4.4. Thermal behavior of sensor

In monitoring applications, in which the strain information is a part of the transduction process, the thermal behavior of the measurement system must be known since most current measurements are done outdoors. This data can be later applied to compensate temperature variation effects. In order to submit the gratings attached to Terfenol-D and nickel rods to a wide temperature range a testing set-up composed by a thermal shaker and a 2000 ml becher with water, where the sensors are immersed (Figure 32), was used.

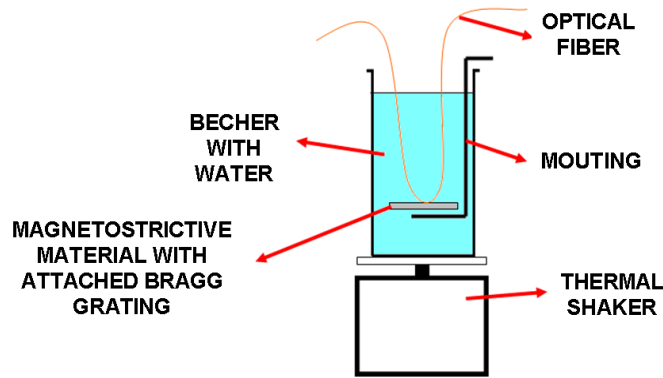


Figure 32. Thermal behavior experiment set-up

Considering that the fixation of the Bragg gratings over the surface of the rods is ideal, the strain over the optical fiber developed during the experiment is due to the magnetostrictive material linear thermal expansion, i.e., ε_m . Thus,

$$\frac{\Delta L}{L_0} = \varepsilon_m = \alpha_M \Delta T \quad (29)$$

where α_M is the MM linear thermal expansion coefficient.

For strain measurements, taking into account the Bragg wavelength expression given by [19]

$$\frac{\Delta \lambda_B}{\lambda_B} = k \cdot (\varepsilon_m + \alpha_S \Delta T) + \frac{1}{n} \frac{\delta n}{\delta T} \Delta T \quad (30)$$

where $\Delta \lambda_B$ is the Bragg wavelength shift, λ_B is the Bragg wavelength at the beginning of the test, k is the gauge factor ($k=0.78$), ΔT is the temperature variation, α_S is the silica thermal expansion coefficient, and $1/n \cdot (\delta n / \delta T)$ is the temperature dependence of the refractive index.

Therefore, using Eq. 29 and 30 one can obtain

$$\frac{\Delta\lambda_B}{\Delta T} = \lambda_B \left(k\alpha_M + k\alpha_S + \frac{1}{n} \frac{\delta n}{\delta T} \right) \quad (31)$$

The theoretical thermal sensitivity of the opto-mechanical sensor is given by Eq 31. For the nickel rod, with $\lambda_B = 1537.547$ nm ($T = 5.6^\circ\text{C}$) and $\alpha_M(\text{nickel}) = 13.3 \times 10^{-6}/^\circ\text{C}$, the sensitivity of the Bragg wavelength as a function of temperature is

$$\frac{\Delta\lambda_B}{\Delta T_{\text{NICKEL}}} = 0.0258 \text{ nm}/^\circ\text{C} \quad (32)$$

Being the magnetostrictive material Terfenol-D, and $\lambda_B = 1539.727$ ($T=5.6^\circ\text{C}$) and $\alpha_M(\text{terfenol})= 12 \times 10^{-6}/^\circ\text{C}$, the sensitivity of the Bragg wavelength as a function of temperature is

$$\frac{\Delta\lambda_B}{\Delta T_{\text{TERFENOL}}} = 0.0242 \text{ nm}/^\circ\text{C} \quad (33)$$

For the nickel rod, admitting a Bragg wavelength infinitesimal variation for an infinitesimal temperature variation, from Eq. 32 we have

$$\begin{aligned} d\lambda_B &= 0.0258 \cdot 10^{-9} dT \\ \lambda_B &= \int 0.0258 \cdot 10^{-9} dT \\ \lambda_B &= 0.0258 \cdot 10^{-9} T + C \end{aligned} \quad (34)$$

where C is the integration constant for the indefinite integral.

Considering the Bragg wavelength just after the stretching process as the initial condition $\lambda_B=1538.019$ nm ($T=24.6^\circ\text{C}$).

Using Eq. 33 one obtain

$$C = 1537.384 \text{ nm.}$$

Hence, the theoretical thermal sensibility for the nickel-based set-up is

$$\lambda_{B(\text{NICKEL})} = 0.0258 \cdot 10^{-9} T + 1537.384 \text{ nm} \quad (35)$$

Repeating this procedure for the Terfenol-D-based set-up, where $\lambda_B = 1540.046$ nm ($T = 23.8^\circ\text{C}$), the obtained value for the integration constant is $C = 1539.470$ nm. Thus,

$$\lambda_{B(\text{TERFENOL})} = 0.0242 \cdot 10^{-9} T + 1539.470 \text{ nm} \quad (36)$$

In Figures 33 and 34 the measured responses, when both sensor heads are submitted to a temperature variation range of approximately 60°C , are presented. For comparison purposes, a tendency line that adjusts the experimental data and the calculated theoretical thermal sensitivity for each developed set-up are also showed.

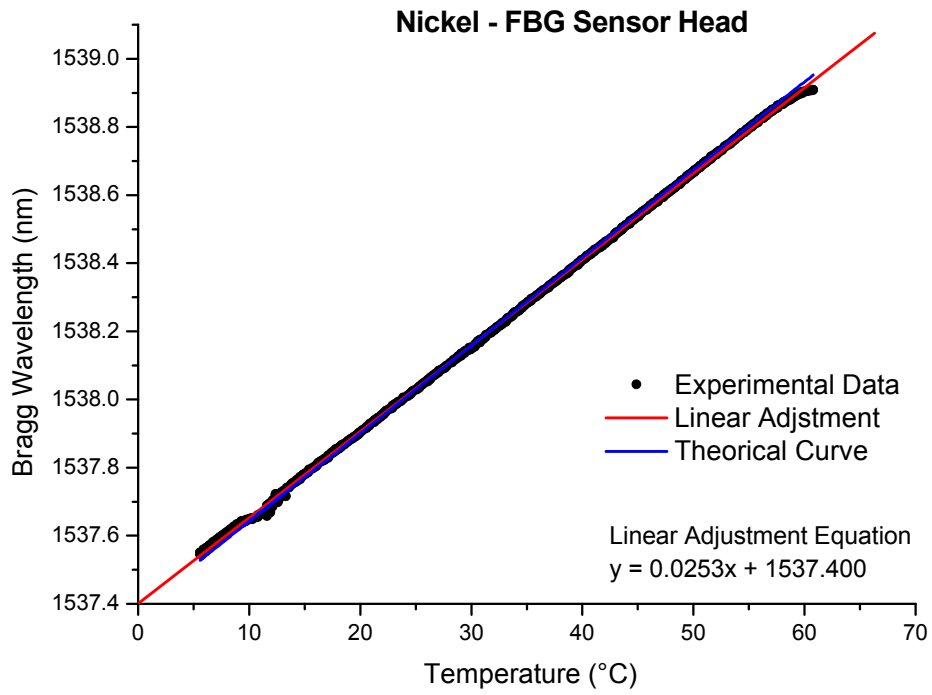


Figure 33. Bragg wavelength as function of temperature for the nickel – FBG sensor head

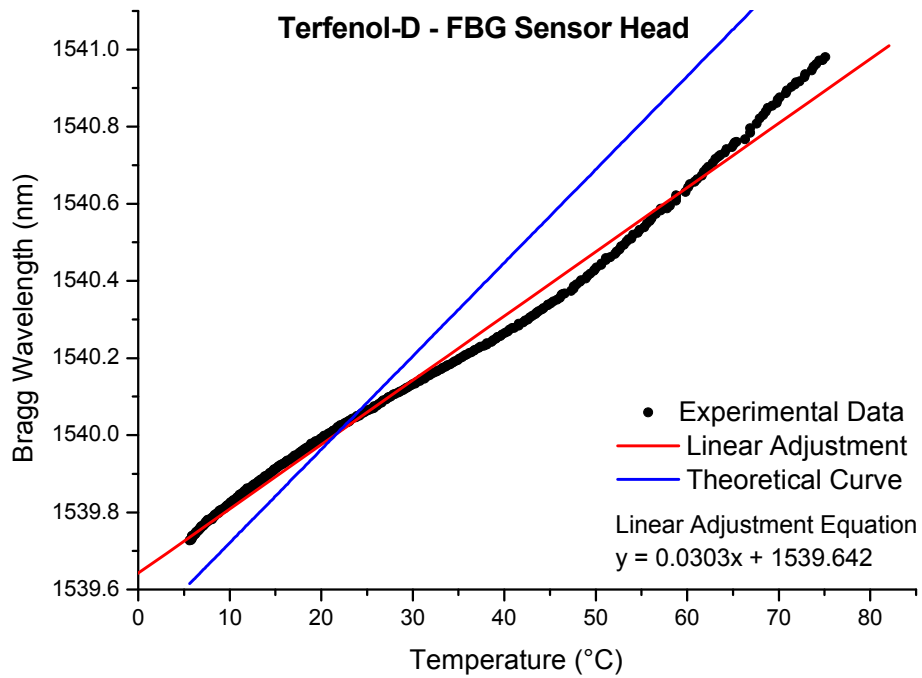


Figure 34. Bragg wavelength as function of temperature for the Terfenol-D – FBG sensor head

4.5. Discussion

The Bragg wavelength for the nickel-based transducer decreases as the current increases, once this material presents a negative magnetostrictive coefficient; whereas the Terfenol-D-based prototype shows a positive magnetostriction (and the Bragg wavelength increases as the current increases).

During the experiments disregarding the temperature effects on the response, the nickel-based transducer showed an average Bragg wavelength shift range of 0.038 nm for a current variation range of 27 A. For the same current range, the Terfenol-D-based transducer showed an average Bragg wavelength shift range of 0.449 nm, approximately one order of magnitude larger than the one showed by the nickel-based transducer. However, considering the temperature effects through the tendency lines obtained during the temperature compensation experiments and showed in Figures 33 and 34, this influence has to be taken into account. Thus, in this case, the nickel-based transducer showed an average Bragg wavelength shift range of 0.063 nm, while the Terfenol-D-based transducer exhibited an average Bragg wavelength shift range of 0.417 nm. When thermal effects are compensated the nickel-based transducer Bragg wavelength shift range is increased, since in this particular situation the heating and the magnetostrictive effects work in opposite directions on the FBG response, i.e., while the current induced magnetic field decreases the read Bragg wavelength, the heating increases it.

Nickel and Terfenol-D are suitable materials to be used in current monitoring transducers; yet, the alloy shows an improved response for a specific current range, since it is a giant magnetostrictive material. The development stages of a complete transducer system include the use of greater DC currents to investigate the saturation region of the materials, and the modeling of the response of the transducers when submitted to different mechanical stresses and magnetic biases in order to determine an optimized sensor set-up for both DC and AC current measurements.

Author details

Regina C. S. B. Allil

Instrumentation and Photonics Laboratory, Electrical Engineering Program, Universidade Federal do Rio de Janeiro (UFRJ), RJ, Brazil

Division of Chemical, Biological and Nuclear Defense, Biological Defense Laboratory, Brazilian Army Technological Center (CTEx) RJ, Brazil

Marcelo M. Werneck, Bessie A. Ribeiro and Fábio V. B. de Nazaré

Instrumentation and Photonics Laboratory, Electrical Engineering Program, Universidade Federal do Rio de Janeiro (UFRJ), RJ, Brazil

5. References

- [1] Stone G C, Overview of Hydrogenerator Stator Winding Monitoring, International Conference on Electric Machines and Drives, -IED, May 1999, 806-808, Seattle, WA.

- [2] Werneck M.M, Allil R.C.S, Ribeiro B. A, Calibration and operation of a fiber Bragg grating temperature sensing system in a grid-connected hydrogenerator, accepted for publication on IET Science, Measurements and Technology in September 2012.
- [3] A. Klimek, Optical Technology: A new Generation of Instrument Transformer, *Electricity Today*, issue 2, 2003.
- [4] S. K. Lee, Electrooptic voltage sensor: birefringence effects and compensation methods, *App. Optics*, 1990, vol. 29, no. 30.
- [5] Emerging Technologies Working group and Fiber Optic Sensors Working Group, "Optical Current Transducers for power systems: a review", *IEEE Trans. Power Delivery*, 9(4), 1778-1788, 1994.
- [6] M. M. Werneck, A. C. S. Abrantes, Fiber-optic-based current and voltage measuring system for high-voltage distribution lines, *IEEE Transactions on Power Delivery* 19 (3): 947-951 Jul 2004.
- [7] B. A. Ribeiro, M. M. Werneck, FBG-PZT sensor system for high voltage measurements, 2011 IEEE Instrumentation and Measurement Technology Conference, 10-12, May 2011.
- [8] Instrument Transformers-Part 5-Capacitor Voltage Transformers, IEC60044-5, 2004.
- [9] B. Ribeiro, M. M. Werneck and J. L. S. Neto, Otimização da demodulação de sinais de um transformador de potencial óptico usando um filtro óptico sintonizável, *Congresso Brasileiro de Automática- CBA*, Sept. 2012.
- [10] D. Reilly, A. J. Willshire, G. Fusiek, P. Niewczas, and J. R. McDonald. A fiber-bragg-grating-based sensor for simultaneous AC current and temperature measurement. *IEEE Sensors Journal*, 2006, vol. 06, 1539–1542.
- [11] F. V. B. de Nazaré and M. M. Werneck. Temperature and current monitoring system for transmission lines using power-over-fiber technology, 2010 IEEE Instrumentation and Measurement Technology Conference. 779 – 784, May 2010, Austin – Texas - USA.
- [12] R. C. S. B. Allil and M. M. Werneck. Optical high-voltage sensor based on fiber Bragg grating and PZT piezoelectric ceramics. *IEEE Transactions on Instrumentation and Measurement*, vol. 60, n. 6, 2118-2125, June 2011.
- [13] E. Hristoforou and A. Ktena. Magnetostriction and magnetostrictive materials for sensing applications. *Journal of Magnetism and Magnetic Materials*, 372 – 378, 2007.
- [14] A. Olabi and A. Grunwald. Design and application of magnetostrictive materials. *Materials and Design* 2008; 469 – 483.
- [15] J. Mora, A. Díez, J. L. Cruz and M. V. Andrés. A magnetostrictive sensor interrogated by fiber gratings for DC-current and temperature discrimination. *IEEE Photonics Technology Letters*, 1680 – 1682, 2000.
- [16] D. Satpathi, J. A. Moore and M. G. Ennis. Design of a Terfenol-D based fiber-optic current transducer. *IEEE Sensors Journal*, 1057 – 1065, 2005.
- [17] J. Mora, Ll. Martínez-León, A. Díez, J. L. Cruz and M. V. Andrés, Simultaneous temperature and ac-current measurements for high voltage lines using fiber Bragg gratings, *Sensors and Actuators A* 125, 313 – 316, 2005.

- [18] G. Engdahl and C. B. Bright, Magnetostrictive Design, in Handbook of Giant Magnetostrictive Materials, G. Engdahl, Academic Press, 207 – 286, 2000.
- [19] M. Kreuzer, Strain measurement with fiber Bragg grating sensors, HBM Deutschland, Darmstadt – Germany.

IntechOpen

IntechOpen